ISSN 1069-3513, Izvestiya, Physics of the Solid Earth, 2011, Vol. 47, No. 5, pp. 379–401. © Pleiades Publishing, Ltd., 2011.
Original Russian Text © D.M. Pecherskii, D.K. Nurgaliev, V.A. Fomin, Z.V. Sharonova, D.M. Gil'manova, 2011, published in Fizika Zemli, 2011, No. 5, pp. 12–34.

Extraterrestrial Iron in the Cretaceous–Danian Sediments

D. M. Pecherskii[a], D. K. Nurgaliev[b], V. A. Fomin[c], Z. V. Sharonova[a], and D. M. Gil'manova[b]

[a] *Schmidt Institute of Physics of the Earth, Russian Academy of Sciences, Bol'shaya Gruzinskaya ul. 10, Moscow, 123995 Russia*
e-mail: diamar1@front.ru
[b] *Kazan Federal University, Kremlyovskaya ul. 18, Kazan, Republic of Tatarstan, 420008 Russia*
[c] *Saratov State University, Astrahanskaya ul. 83, Saratov, Saratov Oblast, 410012 Russia*

Received December 28, 2009; in final form, April 20, 2010

Abstract—The composition and distribution of particles of native iron in eight sections of the Cretaceous–Danian sediments in the Caucasus, Crimea and Kopet Dagh were studied using thermomagnetic analysis up to 800°C. Iron particles are found in 330 of 571 tested samples, their percentage varies from 10^{-5} to 0.05%, and their distribution is bimodal. It was established that the Santonian sediments of the Caucasus and Kara-Kala are enriched with the iron particles; the upper boundary of these sediments is marked by a sharp drop in the iron content at approximately 84 Ma, which coincides with the upper boundary of the Dzhalal hyperchron. The variations in the Curie point of iron from 680°C up to 780°C reflect the fluctuations of the nickel content. A peak of the elevated iron content with nearly constant nickel of 5% was found in all studied sections, i.e., this is a global effect. The global pattern of the distribution and composition of the iron particles clearly indicates that their origin is associated with cosmic dust. At the same time, the particles of Ni–Fe alloy and pure nickel are very rare, and their concentration does not correlate with the content of iron particles. Apparently, there are very few Ni–Fe and pure nickel particles in cosmic dust is very small, and, most likely, the particles of Ni–Fe alloy are mainly due to impact events.

DOI: 10.1134/S1069351311040082

INTRODUCTION

Numerous measurements in the dust clouds, in the atmosphere, in the ice cores from Antarctica and Greenland, and in the oceanic pelagic sediments detected particles of cosmic dust, which contain metallic iron and nickel species. The data on the distribution of these particles both over the Earth's surface and in time are scarce, since only direct methods of detection of such particles were used. These methods require large volumes of material and provide only averaged estimates of the studied parameters. The extensive and rapid information on the distribution of metallic iron, though, can be obtained from the thermomagnetic analysis (TMA) of sediments. TMA is widely applied in the paleomagnetic and rock magnetic studies of different geological objects, including the deposits and sedimentary rocks of different geological age. As the main purpose of these measurements is to estimate the concentration and composition of the major carriers of paleomagnetic record, correspondingly, the temperature of heating in TMA did not usually exceed the Curie point of hematite, i.e., at most approximately 700°C. Thus, the information on the grains of metallic iron was completely excluded in such measurements.

In the rock magnetic studies [Grachev et al., 2009; Pechersky et al., 2006; Pechersky, 2008; Pechersky et al., 2008], in order to trace the spatial and temporal behavior of metallic iron in sediments, thermomagnetic analysis at up to 800°C was applied. In contrast to direct methods, which provide averaged data, here we obtain the information on the iron content as locally as practically in a point, because the weight of the batch of a specimen in TMA does not exceed 0.2 g. By increasing the temperature interval of TMA by 100°C, one can obtain a detailed picture of the particle distribution of metallic iron in space and time.

The main finding of our previous studies is the established enrichment of the Miocene sediments with particles of iron, which was synchronous in two sections: the Khalats (Turkmenia) and Kvirinaki (Georgia) spaced 1500 km apart from each other [Pechersky et al., 2008]. Thus, this phenomenon is most probably global and related with interplanetary space. It does not depend on the local conditions of sedimentation, the composition of sediments, the oxidation-reduction situation, or other factors. The age of this phenomenon is 12.6–12.2 Ma.

The thermomagnetic analysis of sediments on the Cretaceous–Paleogene boundary in Gams (Austria), Tetritskaro (Georgia), Klyuchi and Teplovka (the Volga Region, Russia), and Koshak (Turkmenia) sections [Pechersky, 2008] revealed the widespread occurrence of low-concentration (0.001% at most) metallic iron in the sediments. Besides, the contents of the paramagnetic and magnetic minerals of terrestrial origin were found to be positively correlated with the

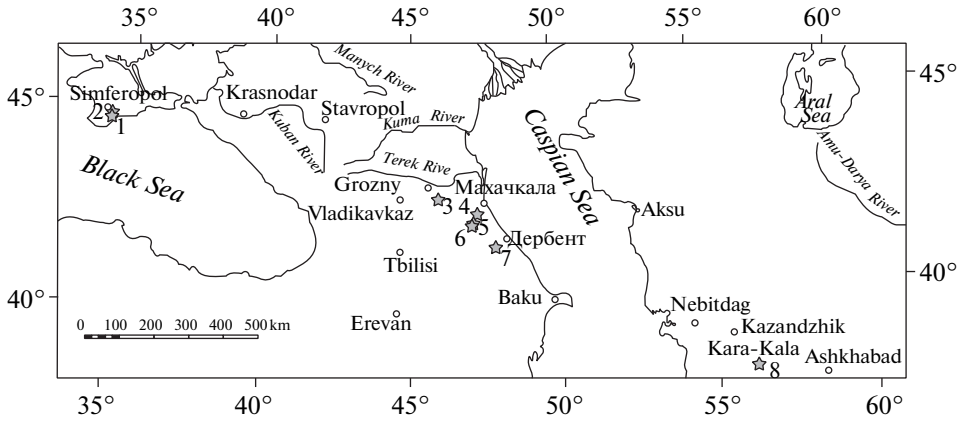

Fig. 1. Layout of the studied sections: (1) Sel'bukhra, (2) Verkhorech'e, (3) Bass, (4) Dzhengutai, (5) Aimaki, (6) Gergebil', (7) Madzhalis, (8) Kara-Kala.

content of the metallic iron, which is explained by the redeposition of the particles of extraterrestrial iron. The observed pattern of the different-intensity positive correlation between the iron and the mentioned minerals reflects different role of redeposition of these minerals.

The present paper addresses the study of distribution of metallic iron in the sediments, which were accumulated during two basically different regimes of the geomagnetic field: (a) the stable state without reversals (the Dzhalal hyperchron, the Barremian–Santonian age, 125–84 Ma) and (b) the unstable conditions with frequent reversals (the Campanian–Danian Tuarkyr and Khorezm superchrons, 84–60 Ma). This is a group of the Caucasus sections, which overlap and supplement each other (Fig. 1). In order to evaluate how "global" the distribution of metallic iron is, the TMA of sediments was carried out in several remote parallel sections of the Kopet Dagh Ridge (the Kara-Kala section) and Crimea (Verkhorech'e, Sel'bukhra) (Fig. 1). Whenever possible, the sections with minimum visible gaps in sedimentation were selected. In order to allow for the role of redeposition in the accumulation of the particles of extraterrestrial iron, attention was paid to the correlations of the iron content with the magnetite, titanomagnetite and ferriferous paramagnetic minerals, whose formation and accumulation, in contrast to those of the metallic iron, are of terrestrialorigin.

THE RESEARCH TECHNIQUE

The rock magnetic tests included measurements of magnetization of the samples and its temperature dependence, i.e., the thermomagnetic analysis. The TMA was carried out with the aid of the Curie express balance [Burov et al., 1986], which enables one to measure the induced magnetization at different temperatures at a rate of heating of 100°C per minute. The thermomagnetic curves after the first and the second heatings up to 800°C are obtained for all samples.

Nickel is known to be the major impurity in the particles of extraterrestrial iron. The Ni content in Fe–Ni alloy can be estimated from the Curie points determined in the TMA. Their conversion into the nickel content allows one to compare the TMA data with the results of the compositional analysis of metallic grains by microprobe and other ways. For this purpose, we assume that the dependence of the Curie point for the iron–nickel alloys is close to linear. Then, the nickel content is determined by a simple formula:

$$\mathrm{Ni}\ (\%) = 0.243(770 - T_c),$$

where 770 is the Curie point of iron, and T_c is the Curie point of the sample.

Let us verify how realistic this assumption is. Close to room temperature, Fe–Ni alloys with less than 30% nickel preserve the ordered bulk-centered lattice (α phase). At higher concentrations of nickel and/or as the temperature increases, the α phase transforms into the γ' phase with the ordered face-centered lattice and into the γ phase with the disordered face-centered lattice [Bozort, 1956; Nagata et al., 1986; *Diagrammy...*, 1997]. The Curie points in such γ and γ' alloys for various reasons substantially deviate from the linear composition–T_c dependence with more frequent underestimation and less frequent overestimation of the true values (Table 1). Thus, apparent Curie points arise, which are due to the tranformation of the α phase into the γ phase upon heating of a sample and the $\gamma \longrightarrow \alpha$ transformation during its cooling. This relates, mainly, to the Fe–Ni alloys of intermediate composition with more than 20% and less than 80% nickel. For these alloys, noticeable divergences of the estimates of the nickel content from the linear T_c–Ni dependence are common (Table 1).

In our case, it is more important not to examine the nature of such deviations, but to explore the possibility

Table 1. Comparison of the compositions of artificial Ni–Fe alloys with the estimates provided by the method of thermomagnetic analysis

Alloy grade	Alloy composition (wt %)	T_c, °C	Ni (%) according to TMA
Vacaperm	Ni100	400	90
cryoperm	Ni90Fe10	430	83
M7904	Ni80, Mo5, Fe15	443	80
Ni80	Ni80Fe20	560	51
Supermuniperm	Ni80Mn5Fe15	410	87
Perm77	Ni77, Mo4, Cu4.4, Fe14	410	87
M75	Ni75, Cr2, Cu5, Fe18	438	81
Ni60	Ni60Fe40	600	41
Carpenter	Ni55Fe45	530	58
AlloyNi50	Ni52Fe48	530	58
AlloyNi50	Ni50Fe50	500	66
Ni50	Ni50Fe50	530	58
M50	Ni48, Fe52	471	73
Nifemax	Ni48Fe52	470	73
Ni40	Ni40Fe60	356	100
Normaperm	Ni36Fe64	240	?
Invar	Ni36Fe64	230	?
Invar	Ni36Fe64	375	96
Invar film standard (1)	Ni36Fe64	250	?
Invar film after stress (2)	Ni36Fe64	400	90
Superinvar	Ni32Co5Fe63	279	?
AlloyNi30	Ni30Fe70	610	39

to estimate the nickel content in the natural particles of Fe–Ni alloys from the Curie point. Here, two questions arise: (1) the extent to which the estimation of the nickel content from the linear T_c–Ni dependence is applicable to the natural meteorites, which contain Fe–Ni alloys of intermediate composition, and (2) the abundance of the particles of the Fe–Ni alloys of intermediate composition in cosmic dust.

To answer the first question, we use the data from the papers [Nagata and Funaki, 1987; Nagata et al., 1986; 1987], where the microprobe data on the composition and the TMA results are presented for a collection of samples of metallic meteorites and metal inclusions in stony meteorites (Table 2). In most cases, the discrepancies between the microprobe and TMA data are rather small. Therefore, on the first approximation, the use of the linear T_c–Ni dependence is admissible for determination of the nickel content from the Curie points. This is all the more justified by the fact that in the particles of metallic iron from the sediments of Fe–Ni alloys, which are of interest to us, intermediate compositions are very rare. To make sure of this, we consider the data in the literature regarding the composition of the metallic particles in cosmic dust, in the ice of the Antarctic and Greenland, in deep-ocean sediments, in the Pleistocene sediments of Canada, in the Eocene limestones of Tuamotu, in the sediments from the region of Tunguska catastrophe, and in the sediments on the Mesozoic–Cenozoic K-T boundary of the Gams section [Brownlee, 1987; Grachev et al., 2009; Parkin, 1964; Shima and Yabuki, 1988]. From the total 84 determinations, in 45% of the cases the particles contained up to 20% nickel; in 46%, the nickel content was 80%; and only in 10%, the nickel content in the particles was intermediate (more than 20% and less than 80%). Thus, the linear T_c–Ni dependence is quite applicable for estimation of the nickel content for most of the particles.

Another difficulty lies in the fact that in the interval between 360°C and 680°C, the Fe–Ni alloy is hardly distinguishable by TMA against the background magnetization contributed by the minerals of the magnetite and hematite group, because the Curie points of the hemoilmenite and titanomagnetite series in this interval of temperature overlap with those of the Fe–Ni alloys. In order to evaluate the compositions of the Fe–Ni alloys, we selected the samples for which the Curie points in the temperature interval of 360–660°C were reproducible upon second heating, and the contribution of these magnetic phases to the value of magnetization practically did not change (Fig. 2). This condition suggests that such samples contain from 100% (T_c = 360°C) to 27% (T_c = 660°C) nickel particles and its iron alloy, because the magnetic min-

Table 2. Comparison of percentage nickel and iron in the meteorites according to the microprobe and TMA data[1]

Meteorite	NiFe	T_c1(%)	T_c2(%)	T_c3(%)	NiFe TMA
St. Catharina	50/50	565			50/50
Twin City	50/50	560			51/49
Toluca (g-lamella)	50/50	580			46/54
Itutinga (g-lamella)	50/50	565			50/50
St. Severin	50/50	565			50/50
Appley Bridge	50/50	565			50/50
Yamato74354	16/84	543(15) 55Ni × 0.15	750(85) 5 × 0.85		13/87
Yamato74362	14/86	545(17) 55Ni × 0.17	740(83) 7		15/85
Yamato74442	28/72	365(7) 98Ni × 0.07	555(21) 52Ni × 0.21	756(72) 3.4Ni × 0.72	21/79
Yamato790964	66/34	560(50) 51Ni × 0.5	610(50) 39Ni × 0.5		45/55
Yamato790448	40/60	575(80) 47Ni	770(20)		47/53
ALH76009	13/87	570(20) 49 × 0.2	765(80) 1.2Ni × 0.8		11/89
San-Cristobal	26/74	565			50/50
Lime Creek	30/70				41/59

Note: NiFe is the content of nickel and iron in a metal part of the meteorite (wt %) according to the data of microprobe analysis, T_c is the Curie point (the fraction of magnetic phase in the value of magnetization, determined from the TMA curve, %, is shown in brackets); NiFe TMA is the total content of nickel and iron determined from the linear dependence T_c–Ni, wt %.)

erals which refer to this interval (pyrrhotines, titanomagnetites, hemoilmenites) are unstable; on being heated up to 800°C, they are oxidized, destroyed, and/or homogenized, which noticeably changes their Curie points and their contributions to the magnetization of a sample.

The contribution of a given magnetic mineral to the magnetization of a sample can be estimated with a relative accuracy of not better than 10%, and, correspondingly, the accuracy in the determination of the concentration of particles of iron and alloy is no better. These values are quite sufficient for us, because the concentration of the iron particles in the studied samples varies from 10^{-5}% and even lower (undetectable by TMA) up to 10^{-2}% and even higher. The determination accuracy of the Curie point is approximately 5–10°C, which corresponds to the determination accuracy of the nickel content in alloy of 1–2%, i.e., we may accept that the error of each determination does not exceed 2%. The disadvantages of application of the linear T_c–Ni dependence and the accuracy of TMA are overweighted by the simple procedure of preparation of specimens and their thermomagnetic analysis, as well as by the rapid and mass obtaining of the data.

For evaluating the concentration of magnetite, titanomagnetite, iron, and Fe–Ni alloy in the samples, the contribution of the given magnetic mineral to the value M_i was determined according to the curve $M_i(T)$, and this value was divided by the specific saturation magnetization of this mineral. The following values of M_s were assumed: for magnetite and titanomagnetite, taking into account their Curie points varying from 550 to 580°C, ~90 A^2/kg; for iron, whose Curie point varies from 700 to 780°C, ~200 A^2/kg. In order to evaluate the concentration of iron and nickel in the Fe–Ni alloy, it was assumed that the saturation magnetization of nickel (M_s = 56.7 A^2/kg) and iron (M_s = 212 A^2/kg) are linked through a linear relation:

$$M_s\,(\text{Fe–Ni alloy}) = 56.7 + 0.37(T - 360)$$

The paramagnetic magnetization of the studied samples is determined from the magnetic measurements: $M_p = 1.378\,(M_{20} - M_{800})$, where M_p is the paramagnetic magnetization at room temperature in the field of 500 mT, M_{800} is the diamagnetic magnetization at room temperature in the field of 500 mT (the diamagnetic magnetization is almost temperature independent), and M_{20} is the magnetization of a sample measured at room temperature in the field of 500 mT. If the TMA curve is hyperbolic, when the contribution of magnetic minerals in M_{20} is negligible, it is the sum of the paramagnetic and diamagnetic magnetizations. If the TMA curve is parabolic, the value of M_p is determined according to the Curie–Weiss law as M_{800} 1075 K/295 K; M_{800}. is the the magnetization of a sample at a temperature of 800°C measured in the same field as M_{20}. The factor 0.274 M_p is the ratio of temperatures 295 K/1075 K (the Curie–Weiss law). Actually, the value of paramagnetic magnetization is determined by the sum of the paramagnetic iron-containing minerals.

Upon heating, the samples of the studied collections frequently exhibited a TMA peak above 500°C with a maximum at 510–530°C. The descent of the M_i (T) curve, which follows the peak, ends at the Curie point at 590–595°C, which indicates that this is the cation-deficient magnetite that emerged in the course of heating in the laboratory. The appearance of mag-

netite upon heating above 500°C can serve as the diagnostic feature of sulfides (pyrite and arsenopyrite) [Novakova and Gendler, 1995]. The amplitude of the peak approximately indicates the lower limit of the concentration of supfides like pyrite. Further in the text, it will be referred to as "pyrite" since more accurate diagnostics are not available.

The successions of sediments in all sections were converted into time to make them convenient for comparison. It was done in the following way: it was assumed that in the interval corresponding to the thickness of each stratigraphic unit the sedimentation was uniform and occurred at a constant rate. Accordingly, the rate of sedimentation was determined as the time (duration) of the given stratigraphic unit divided by its thickness, and then, for each point of sampling, the age of the sample was determined by multiplication of the distance (thickness) to the boundary of the layer by the rate of sedimentation. The age of the stratigraphic units was taken according to the geological time scale-2008 [Gradstein et al., 2008].

THE STUDY RESULTS FOR DIFFERENT SECTIONS

Caucasus

The Upper Cretaceous deposits of the Calciferous Dagestan extend across the entire territory of Ciscaucasia, forming a continuous strip here. In this region, the Aimaki, Dzhengutai, Madzhalis, Bass, and Gergebil' sections were studied (Fig. 1). The detailed description of the sections is presented in the works [*The Upper* ..., 1986; Pergament, 1978; Rengarten, 1975, etc.]. Here, below we briefly outline the composite section of the Calciferous Dagestan.

The Cenomanian sequence is represented here by alternating layers of gray limestones and green-gray marls with a total thickness up to 90 m. An alternation of black, greenish gray and white limestones and marls with a thickness of 37–42 m forms the Lower Turonian. The Upper Turonian is composed of the green-gray, pink and red-brown marls and limestones. The thickness of the Upper Turonian sediments is up to 54 m. The Coniacian rocks are lithologically of the same type as the Upper Turonian. The thickness of this sequence is up to 110 m. The Santonian is represented by gray limestones and marls up to 80 m thick. The Campanian is composed of white layered limestones and light grey shaly limestones with a thickness of 200–460 m. The Maastrichtian sequence is represented by gray marls; the thickness is 120–400 m. The Danian sediments concordantly overlie the Maastrichtian formations and are composed of shaly limestones interbedded by marls. The thickness of this portion of the section is approximately 170 m. In the lower part of this sequence, the limestone landslide pebble is found.

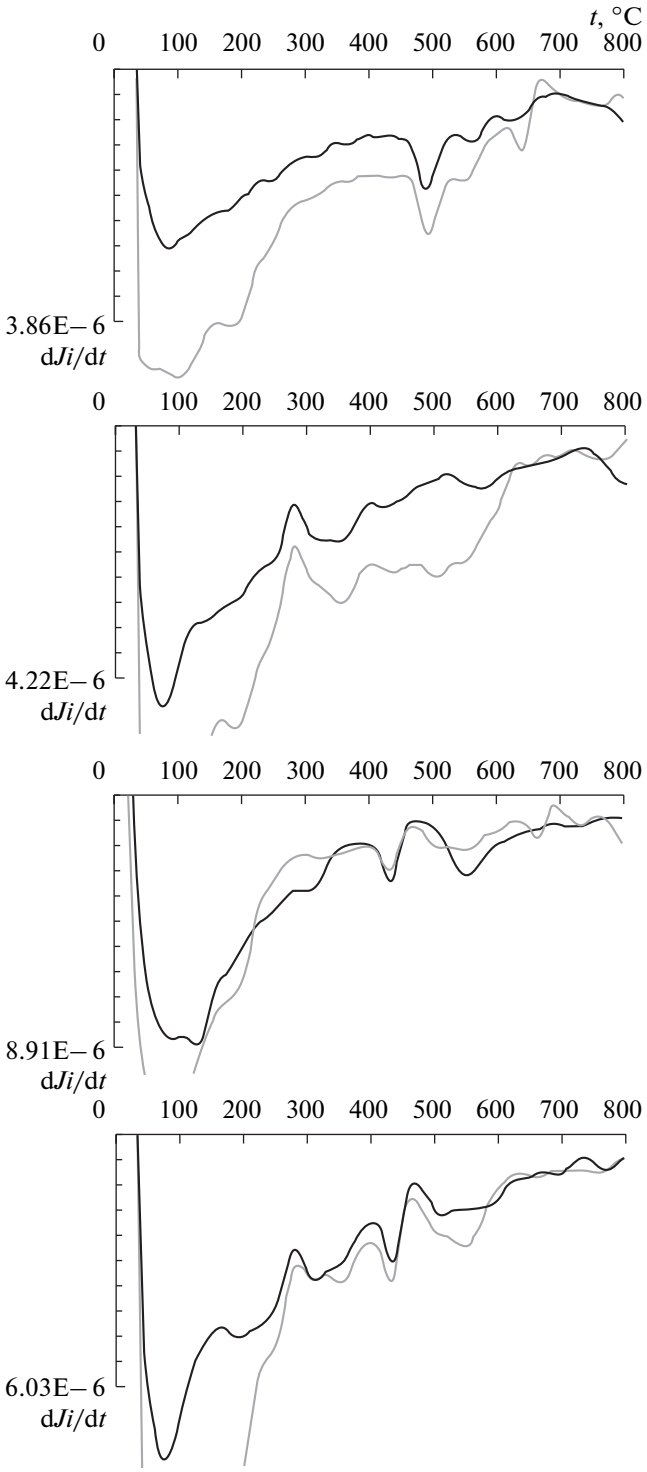

Fig. 2. Examples of the curves of differential thermomagnetic analysis (DTMA), in which the magnetic phase referred to the Fe–Ni alloy is present: (a) sample 2029-100 (Bass, T_c = 500°C); (b) sample 2029-110 (Bass, T_c = 365°C); (c) sample 2035-7 (Aimaki, T_c = 445°C); (d) sample 2562-4 (Sel'bukhra, T_c = 440°C). The solid curve represents the first heating, the thin curve represents the second heating.

Table 3. Characteristics of the Ni–Fe alloy[2]

Section	Sample	T_c	%Ni	NiFe	Fe	MT	Ma	N	N(Fe)	N(NiFe)
Aimaki	2035-7	450	78.5	0.11	0.09	1	99.06	112	60	1
Bass	2029-110	370	97	0.1	0	0.4	62.78	104	57	2
	2029-100	500	66.6	0.08	0.01	0.3	64.96			
Gergebil'	2038-206	460	76.2	0.12	0	0.9	110.13	44	36	4
	83	380	93	0.4	0	2	123.8			
	31	455	77.4	0.3	0	24.5	127.36			
	6	360	100	0.35	0	23.2	129.43			
Madzhalis	2061-48	440	81	0.02	0	0.7	86.1	57	39	2
	37	365	98	0.05	0	0.3	87.2			
Dzhengutai	2057-78	445	79.7	0.04	0.8	1.28	84.4	13	8	2
	19	455	77.4	0.03	0.03	1.3	89.5			
Kara-Kala	2048-128	455	77.4	0.13	0.04	6.3	69.72	181	98	3
	138	450	78.5	0.05	0.03	2	70.64			
	175	440	81	0.01	0.01	8.6	74.5			
Sel'bukhra	2562-4	440	81	0.1	0.14	0.8	99.02	36	27	2
	2562-7	440	81	0.07	0.12	0.75	98.44			

Note: T_c is the Curie point of the particles of Ni–Fe alloy; %Ni is the nickel content in the alloy determined from the Curie point; NiFe is the content of the particles of Ni–Fe alloy in the sample, 10^{-3}%; Fe is the iron content in the same sample, 10^{-3}%; MT is the content of magnetite and titanomagnetite in the same sample, 10^{-3}%; Ma is the age of sediment at the locality of sampling, Ma; N is the total number of TMA-tested samples in the section; N(Fe) is the number of samples in which iron was detected; N(NiFe) is the number of samples in which Ni–Fe alloy was detected.

Aimaki

Near the Aimaki and Okhli localities (Dagestan) (Fig. 1), an almost continuous sequence of sediments from the Cenomanian to the Danian Stage with a total thickness of 1015 m outcrops in a series of exposures. The gaps in sedimentation are revealed on the Maastrichtian–Danian and the Lower Turonian–Upper Turonian boundaries. The sediments are presented exclusively by carbonate rocks with shaly impurities (limestones and marls).

Of most interest for our study is to examine the distribution of metallic iron throughout the section (Fig. 3a, 3f, and 3g). Iron in excess of 10^{-5}% (Fig. 3a), reaching 0.0085%, is found in 60 samples of 112 studied. The Curie point varies from 755°C to 780°C and is 755°C on average (Fig. 3g). Correspondingly, the nickel percentage reaches 17% and is about 4% on average. The magnetic phase with the signs of Fe–Ni alloy is identified in one sample only (Table 3).

The iron is nonuniformly distributed throughout the section. Its highest content (0.0085%) is observed in the Late Cenomanian deposits within a narrow interval of 890–877 m (Fig. 3a), which corresponds to the age of 95.7–95 Ma (Fig. 3f). Higher in the succession, an increased iron content of $0.3–0.8 \times 10^{-3}$% is identified at a depth from 710 to 635 m (87–84.6 Ma, Figs. 3a, 3f). The iron content drops approximately at the upper boundary of the Dzhalal hyperchron.

Obviously, the fraction of clay materials is ensued by the corresponding content of paramagnetic minerals, which manifests itself in the variations of the paramagnetic magnetization (Fig. 3c). Magnetite is pervasive; its Curie temperature is $T_c = 560–640$°C, more often $T_c \geq 600$°C, which indicates the single-phase oxidation of magnetite. Titanomagnetite is more rare, its Curie temperature $T_c = 510–550$°C; in particular, such Curie points appear upon heating the sample up to 800°C, obviously, due to the partial homogenization of the titanomagnetite grains which underwent heterophase oxidation. The concentrations of magnetite (+ titanomagnetite) vary from 10^{-4}% to 10^{-2}% (Fig. 3b) and noticeably correlate with M_p (Fig. 3c), the coefficient of linear correlation being 0.662 (Table 4). This implies joint accumulation of clay material and magnetite. In all samples, the magnetic phases with $T_c = 70–140$°C, and less frequently 310–340°C and 410–460°C are revealed. Since in most cases these phases are preserved (at least, partially) upon heating up to 800°C , these are precisely the Curie points and they, most likely, correspond to the

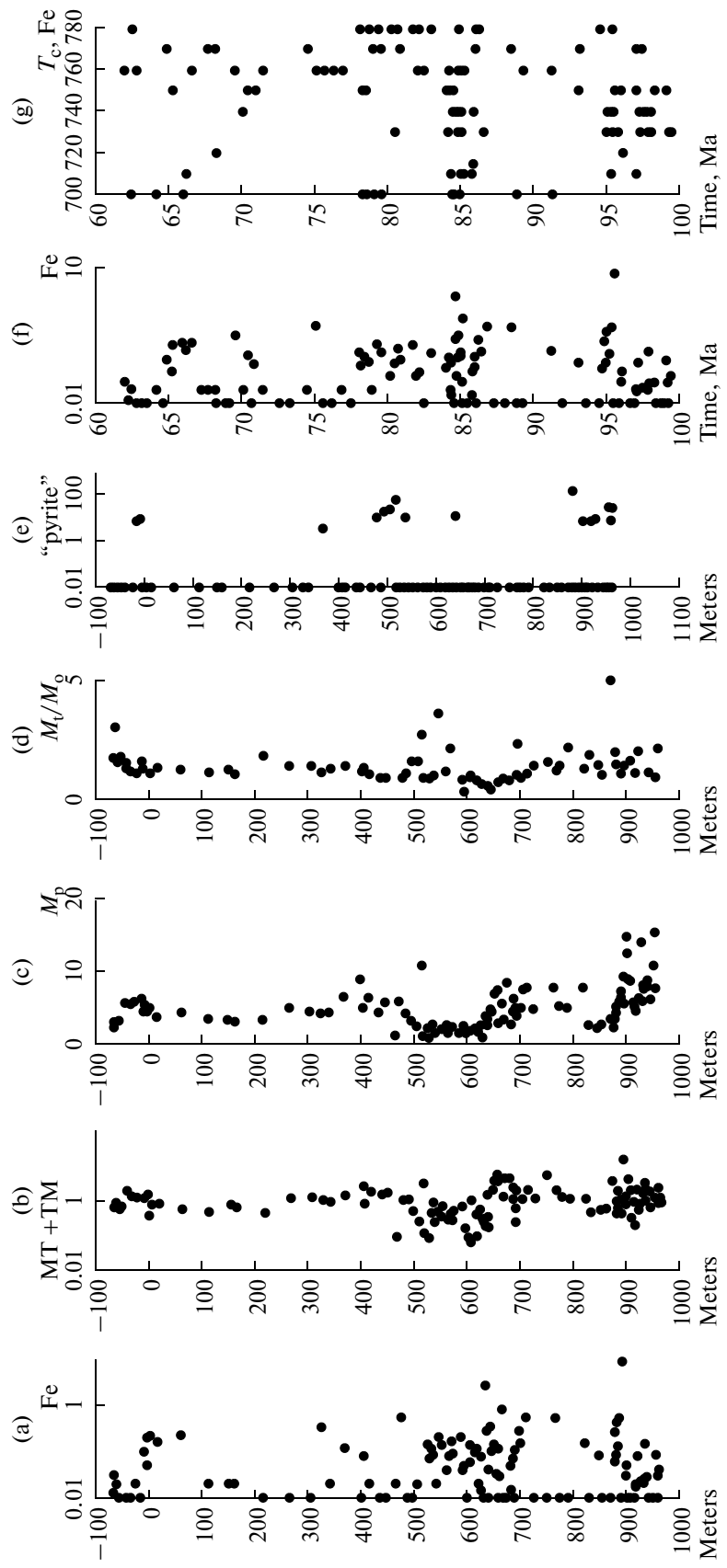

Fig. 3. The Aimaki column: (a) iron content, 10^{-3}%; (b) content of magnetite + titanomagnetite, 10^{-3}%; (c) fraction of paramagnetic magnetization M_p, 10^{-3} A^2/kg; (d) the ratio of the magnetization value uponheating of the sample up to800°Cto its initial value; (e) the amplitude of the peak in the TMA curve for 510–530°C (the percentage relative to the initial magnetization of the sample), which reflect the formation of magnetite when "pyrite" is oxidized as a result of the heating of the sample; (f) and (g) the time distributions of the iron content and of the Curie points of iron, respectively.

Table 4. Coefficients of linear correlation

r	Aimaki	Bass	Dzhengutai	Madzhalis	Gergebil'	Kara-Kala	Ver-chorech'e	Sel'bukhra
M_p-MT	0.37	0.952	0.372	0.229	0.442	0.622	–0.347	0.377
$\log M_p$ - (log M)T	0.4	0.725	0.367	0.465	0.548	0.635	0.028	0.507
M_p-Fe	0.083	–0.101	0.482?	0.265	0.209	0.354	–0.157	0.409
$\log M_p$-log Fe	–0.024	0.304	0.268?	0.322	0.172	0.326	0.05	0.436
MT-Fe		–0.077	0.516?	0.012	–0.041	0.355	–0.319	0.737
(log F)e - (log M)T	0.147	0.18	0.174?	–0.094	0.108	0.272	–0.611	0.616
pik-M_p		0.433				0.049		
pik-MT		0.331				0.186		
pik-Fe		–0.097				0.029		

Note: M_p is the paramagnetic magnetization in the field of 500 mT; MT is the content of magnetite and titanomagnetite; Fe is the content of metallic iron; pik is the amplitude of a peak in the TMA curve, which reflects the transformation of "pyrite" into magnetite in the course of laboratory heating of the sample.

varieties of iron spinels and hemoilmenites [Grachev et al., 2009].

The decrease in the iron content on the upper boundary of the Dzhalal hyperchron correlates with the reduction in magnetite and paramagnetic minerals, which we associate with the redeposition of iron together with the other minerals of terrestrial origin [Pechersky, 2008]. Another interval between 60 and 10 m (66.6–65.2 Ma) marked by the increased iron content which drops on the Maastrichtian–Danian boundary, in contrast to the previous decrease, is not displayed in the behavior of M_p.

In a number of horizons of the section, especially in the intervals 475–545 m and 900–950 m, the peaks in the TMA curve above 500°C (Fig. 3e) mark the "pyrite". Its appearance does not correlate with contents of iron, magnetite, and paramagnetic minerals (Table 4), which emphasizes its more probable authigenic origin, younger than the deposition of sediments. It is rather doubtful that the grains of pyrites had been preserved during the accumulation of sediments. The magnetization of samples upon their heating up to 800°C is close to unity or increases. The latter is partly due to the presence of "pyrite", whose oxidation during the heating results in the formation of magnetite and, correspondingly, in the increase of magnetization (Fig. 3d). In the other cases, the growth in magnetization is most likely connected with homogenization of hemoilmenite [Grachev et al., 2009].

Dzhengutai Approximately 15 km to the north of the Aimaki section (Fig. 1), along the highway which intersects the Chabanskii Ridge, on the way southward from the Upper Dzhengutai to the Levashi settlement, the carbonate deposits from the Upper Turonian (above the gap) up to the Santonian outcrop, following the corresponding interval of the Aimaki section. The thickness of the deposits is 100 m, which is noticeably lower than in the Aimaki section where the Upper Turonian–Santonian sequence is 250 m thick.

Iron is identified in eight samples of thirteen. An interval 7–18 m in thickness (Fig. 4a) or 84.4–85.6 Ma (Fig. 4e) in age is clearly distinguished where the iron content attains 0.45×10^{-3}%. The Curie points of iron vary from 700°C to 780°C with the mean T_c = 735°C, which corresponds to up to 17% (8.5% on average) nickel concentration. The magnetic phases with indications of Fe–Nialloy are detected in two samples (Table 3). The horizon 84.4–85.6 Ma practically replicates the iron-enriched horizon of the Aimaki section, which suggests that the enrichment with iron is regional. It is very important to highlight this fact, because this horizon approximately corresponds to the upper boundary of the Dzhalal hyperchron.

Throughout the section, the magnetic phases with T_c = 80–110, 200–270, and 410–460°C are abundant. Most probably, these are iron spinels, hemoilmenites;

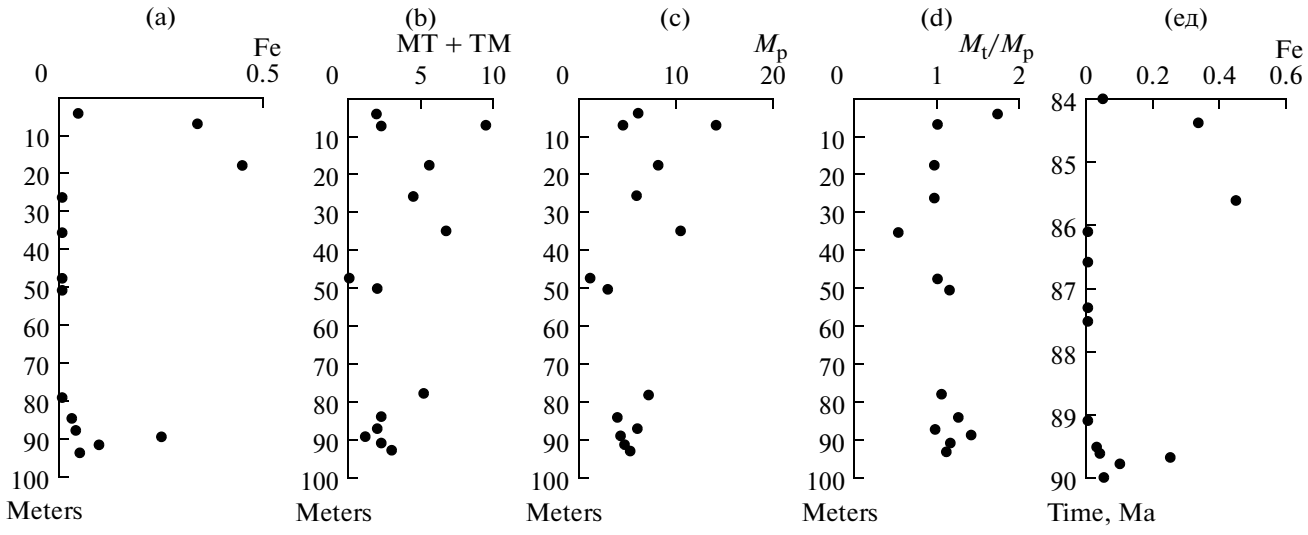

Fig. 4. The Dzhengutai column: (a) iron content, 10^{-3}%; (b) content of magnetite + titanomagnetite, 10^{-3}%; (c) fraction of paramagnetic magnetization M_p, 10^{-3} A^2/kg; (d) the ratio of the magnetization value after the heating of the sample up to 800°C to its initial value; (e) the time distribution of iron.

the Curie points (410–460°C), most likely, correspond to Ni–Fe alloy rather than to titanomagnetite, which oxidates to magnetite uponheating up to 800°C . None specimens contain magnetite with $T_c = 580$°C , but all contain the cation-deficient magnetite with $T_c = 610$–640°C, which is partially reduced to the magnetite with $T_c = 560$–575°C upon heating. This indicates that the conditions in the sediments of the section were highly oxidizing, which led, in particular, to the low-temperature oxidation of magnetite.

The iron content practically lacks correlation with the magnetite content ($r = 0.174$, Table 4); therefore, here we may speak of the primary accumulation of iron rather than of its redeposition. No "pyrite" has been identified in the Dzhengutai section, which distinguishes it from the Aimaki section.

Madzhalis. Sixty six kilometers southeast from the Aimaki section (Fig. 1), in the cliff faces of the Ullu-Chai river in the neighborhood of the Madzhalis settlement, the section of limestones outcrops, which echoes the Dzhengutai section from the gap in the bottom part of the Upper Turonian to the tops of the Santonian. The Madzhalis section has practically the same thickness (120 m) as the Aimaki section.

Iron is identified in 39 samples of 57 tested. The iron distribution in the two sections noticeably differs (Figs. 4 and 5). The iron content widely varies from less than 10^{-5}% to 10^{-3}%, with the highest iron content up to 0.6×10^{-3}% being noted in the interval 81–114 m (Fig. 5a), or 87.8–90.8 Ma (Fig. 5e). The Curie points of iron vary from 690°C to 780°C (Fig. 5f) about the mean Curie temperature $T_c = 735$°C, which corresponds to up to 19% nickel content (on average, about 9%). Signs of Fe–Ni alloy are identified in two samples (Table 3).

The upper boundary of the Dzhalal hyperchron is poorly expressed in the section: in the interval of 84.6–84.5 Ma, the iron content rises up to 0.2×10^{-3}% (Fig. 5).

Both the unoxidized and the cation-deficient magnetite are present, which is evident from the variations of the Curie point from 560°C to 660°C. Titanomagnetite is also detected here; its Curie point varies within the range 490–550°C and is lowered after heating, thereby reflecting partial homogenization of the decomposed grains of titanomagnetite. The concentrations of magnetite (with titanomagnetite), just as in the Aimaki section, vary from 10^{-4} to 10^{-2}% (Fig. 5b) and exhibit noticeable correlation with M_p (Fig. 5c). In contrast to the Aimaki and Dzhengutai sections, in the Madzhalis section, a smooth decrease in the contents of magnetite and paramagnetic minerals is clearly traced from the bottom to the top, which agrees with the smooth reduction in the ratio of magnetization before and after heatingM_t/M_o (Fig. 5). Everywhere throughout the section, the magnetic phases with $T_c = 80$–110, 200–270, and 410–460°C are identified. Most probably, these are iron spinels, hemoilmenites and, possibly, Fe–Ni alloy. The same as in the Aimaki section, the "pyrite" is present here at horizons of 4 m (83.66 Ma), 35.5 m (85.4 Ma), and 40 m (85.53 Ma). The iron content is practically uncorrelated with the contents of terrestrial minerals (Table 4).

Gergebil'. The section located near the Gergebil' settlement closer than 5 km southwest from the Aimaki settlement (Fig. 1) extends to the Aimaki section from below, thereby augmenting it from the Albian to the Barremian. The stratification of the section is given according to Yu.P. Smirnov [*Melovye...*, 1980]. From bottom to top, three members are identified in the section: (1) Aleurolite shale member is composed

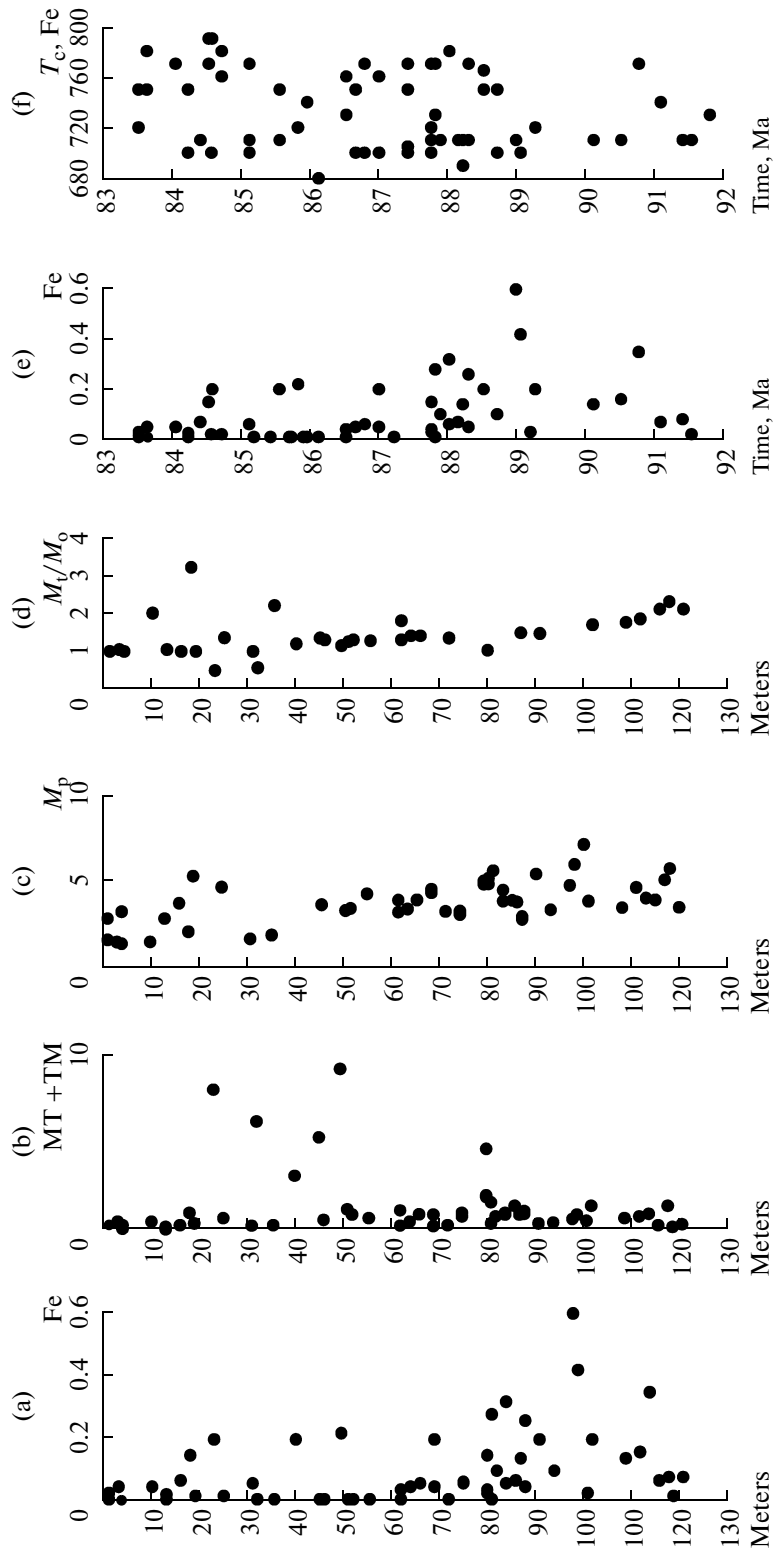

Fig. 5. The Madzhalis column: (a) iron content,10^{-3}%; (b) content of magnetite + titanomagnetite, 10^{-3}%; (c) fraction of paramagnetic magnetization M_p, ^{2}A^2/kg; (d) the ratio of the magnetization value after the heating of the sample up to 800°C to its initial value; (e) the amplitude of the peak in the TMA curve for 510–530°C (the percentage relative to the initial magnetization of the sample), which reflects the formation of magnetite when "pyrite" is oxidized as a result of the heating of the sample; (f) and (g) the time distributions of the iron content and of the Curie points of iron, respectively.

of grey-colored aleurolites, clays, and fine-grained sandstones abundantly interbedded with aleurolite–shell deposits in the lower part of the unit. In the upper part of the member, several continuous horizons of concretions with a size of 0.3–0.5 m are seen. The thickness of the unit is 260 m. (2) The aleurolitic member is represented by the alternation of gray shaly aleurolites and calciferous clays with numerous horizons of concretions of different sizes (0.3–3 m). The visible thickness of the member is 275 m. Further, there is a gap in the outcrop with a length of 8 m. (3) The marly–clay unit is formed by fine interbedding of light marls and dark gray clays. The bottom part of member (1) with a thickness of 181 m refers to the Barremian. Its middle part with a thickness of about 40 m, bounded from the bottom by the phosphorite horizon and from the top by the horizon of concretions, relates to the Lower Aptian. The 39-m-thick upper part of member (1) and the major part of member (2) with a thickness of 195 m refer to the Middle Aptian. The upper part of member (2) corresponds to the Upper Aptian. The interface between the Middle and the Upper Aptian is hidden in the gap of the exposure. The visible thickness of the Upper Aptian sediments is 78 m. The Albian is represented by the lower part of member (3) with a visible thickness of 96 m.

TMA revealed iron in 36 of 44 studied samples of the the Barremian–Albian deposits.The iron content varies from below 10^{-5} to 0.003% (Fig. 6a). The Curie points of iron vary from 710°C to 780°C (Fig. 6g), the mean Curie temperature is T_c = 740°C, which corresponds to nickel content of up to 15% with an average content of 7.5%. In four samples, traces of Fe–Ni alloy were detected (Table 3).

There are several intervals in the sequence where the relative enrichment with iron exceeds 0.001%, namely, 690–687 m (128.1–128 Ma), 410–338 m (118.7–116.1 Ma), 208–184 m (110.06–107.17 Ma), and 132–123 m (100.7–99.7 Ma) (Figs. 6a and 6f). These intervals match neither with the stratigraphic nor with the lithologic boundaries. The bottom boundary of the Dzhalal hyperchron (~125 Ma) is not recognized; possibly, a certain decrease at a level of 122 Ma rerers to it (Fig. 6f).

The distribution of paramagnetic minerals (M_p) obeys the lithological control: from below up to a thickness of approximately 450 m (about 117 Ma) the sandy argillaceous section is characterized by the increased variable M_p, above which M_p smoothly decreases probably as the fraction of clay material increases up to the appearance of marls. In the upper part of the latter (the Upper Albian) M_p increases (Fig. 6c). Within the Barremian–Aptian sequence, the content of magnetite (+ titanomagnetite) smoothly decreases from approximately 0.05%–0.02% to 0.001%, following to some extent the behavior of M_p, whereas in the Albian marls the content of magnetite sharply rises to exceed 0.1% (Fig. 6b). This distinguishes the Albian marls from those of the Upper Cretaceous, which are much poorer in magnetite (Figs. 3b, 4b, 5b, and 6b). Approximately one-half of the tested samples contain magnetite with T_c = 560–580°C and in one-half of the samples the cation-deficient magnetite with T_c > 600°C is detected; in 12 samples titanomagnetite is also present with T_c = 480–550°C, and, frequently, hematite is found. Similar to the Upper Cretaceous deposits, in the Gergebil' sediments the magnetic phases with T_c varying from 80°C to 450°C are very common. In the different horizons of the section, "pyrite" is identified (Fig. 6e), whose presence does not correlate with any other minerals and lithologic features of the section.

The distribution of iron throughout the section is not the result of redeposition, which follows from the lack of its correlation with the terrestrial minerals (r = 0.11 and 0.17, Table 4).

Bass. A continuous section of carbonate deposits of the Turonian to Danian age with a total thickness of 1135 m is located approximately 100 km west–northwest of Aimaki (Fig. 1). This section extends along the valley of the Bass River in the neighborhood of the Makhkety village (Chechnya). It is composed of predominant limestones and less frequent argillaceous limestones and marls.

TMA revealed iron in 57 of 104 samples, and only in two of them traces of Fe–Ni-alloy were detected (Table 3). The Curie points of iron vary from 690°C to 780°C (Fig. 7g), and the mean Curie temperature is T_c = 740°C, which corresponds to up to 19% nickel with the mean value 7%. A sufficiently large interval with relatively higher iron content is identified from 634 m to 200 m (87–72 Ma) (Fig. 7f). Within this range, a narrow interval (84.4–83.6 Ma) is distinguished, which is consistent with the Aimaki section (Fig. 3e) and with the Dzhengutai section (Fig. 4e). Also, several bursts of relatively increased iron content at 80.3 Ma (1.2×10^{-3}%) and 73 Ma (1.5×10^{-3}%) are notable (Fig. 7f).

Similar to the other Upper Cretaceous deposits, in the sediments of the Bass section, the magnetic phases with T_c varying from 80°C to 450°C are ubiquitous. Both the unoxidized magnetite (more frequently in the upper part of the section) and the cation-deficient magnetite (clearly predominant in the lower half of the section) are present, which is evident from the variations in the Curie point from 560°C to 660°C. Titanomagnetite is much rarer, and its Curie temperature is T_c = 460–550°C. The content of magnetite + titanomagnetite noticeably correlates with the content of paramagnetic minerals (r = 0.927, Table 4, Fig. 7b and 7c) and to a lesser degree with the "pyrite" content (Fig. 7e) and with the M_t/M_0 ratio (Fig. 7d). This common correlation is most prominent in the intervals of increased magnetite and paramagnetic mineral content, which is due to the increased "pyrite" content. This is a paramagnetic mineral, and under natural conditions it is partially oxidized with the formation of magnetite; in turn, in the course of laboratory heating,

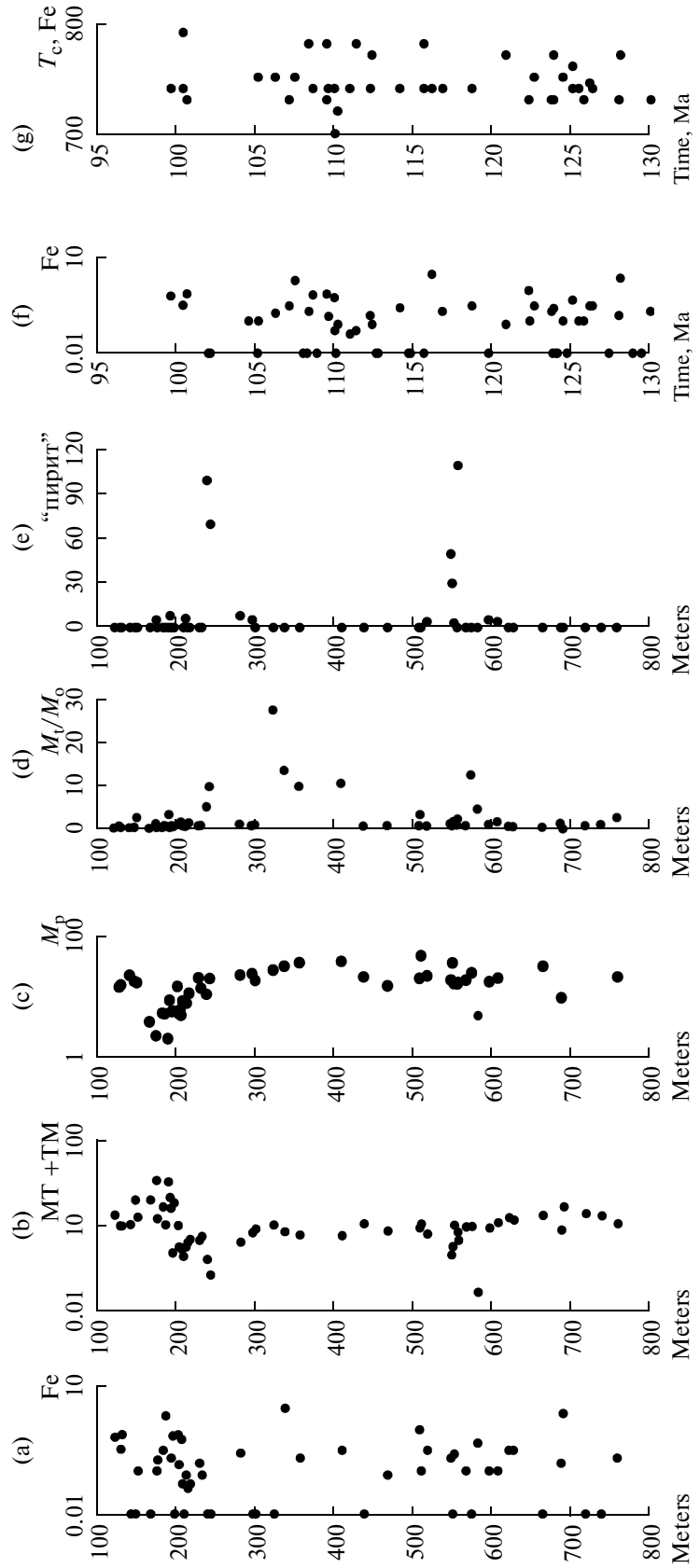

Fig. 6. The Gergebil' column: (a) iron content, 10^{-3}%; (b) content of magnetite + titanomagnetite, 10^{-3}%; (c) fraction of paramagnetic magnetization M_p, 10^{-3} A^2/kg; (d) the ratio of the magnetization value after the heating of the sample up to800°Cto its initial value; (e) the amplitude of the peak in the TMA curve for 510–530°C (the percentage relative to the initial magnetization of the sample), which reflects the formation of magnetite when "pyrite" is oxidized as a result of the heating of the sample; (f) and (g) the time distributions of the iron content and of the Curie points of iron, respectively.

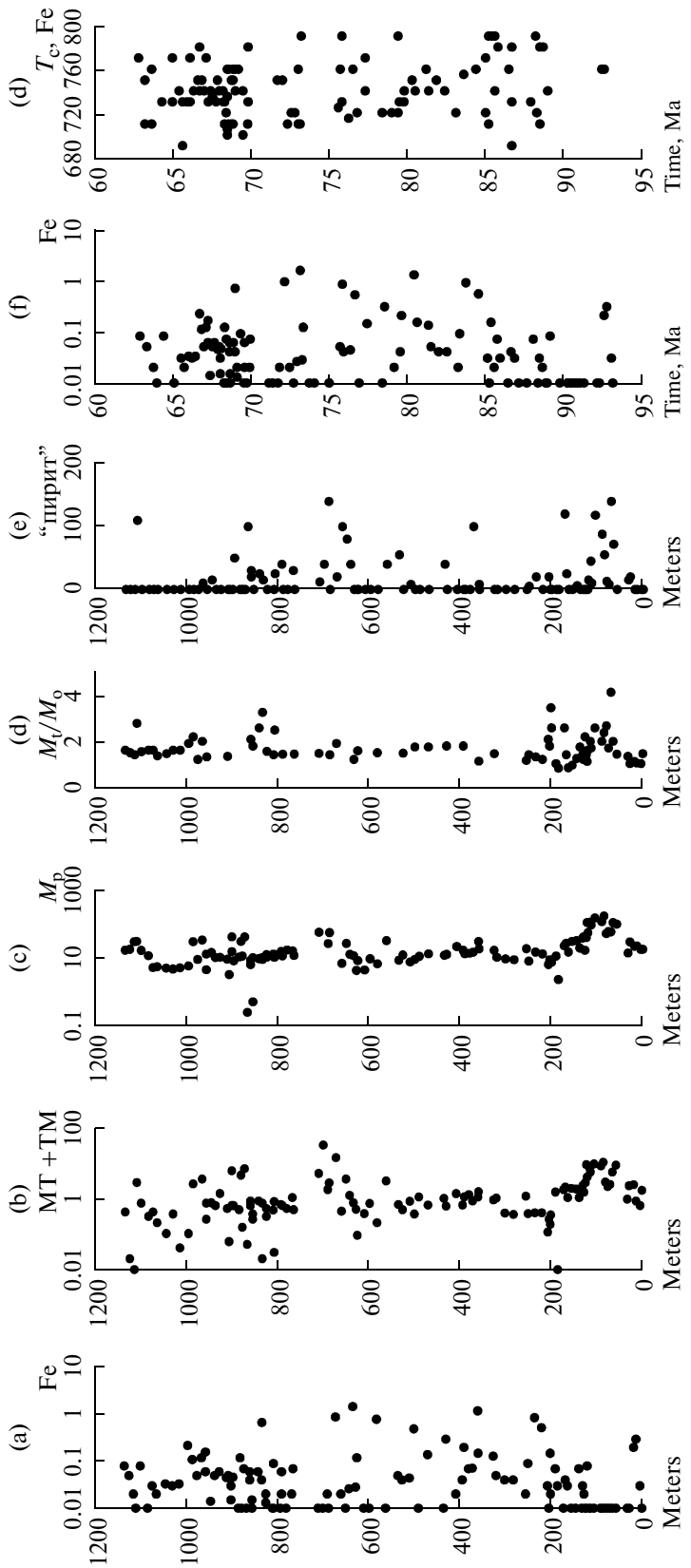

Fig. 7. The Bass column: (a) iron content, 10^{-3}%; (b) content of magnetite + titanomagnetite, 10^{-3}%; (c) fraction of paramagnetic magnetization M_p, 10^{-3} A^2/kg; (d) the ratio of the magnetization value after the heating of the sample up to 800°C to its initial value; (e) the amplitude of the peak in the TMA curve for 510–530°C (the percentage relative to the initial magnetization of the sample), which reflects the formation of magnetite when "pyrite" is oxidized as a result of the heating of the sample; (f) and (g) the time distributions of the iron content and of the Curie points of iron, respectively.

"pyrite" is oxidized to magnetite, which leads to the increase in the M_t/M_0 ratio; all this eventually gives rise to their correlation. The intervals enriched with "pyrite" do not manifest themselves in the lithology; they correspond to the uniform limestone members.

The distribution of iron shows that it is not related either to the magnetite or to the "pyrite", which is evident from the lack of a correlation or weak correlation between these quantities (Table 4, Fig. 7); i.e., the deposition of iron can be regarded as primary.

Kopet Dagh. *Kara-Kala*. In order to reveal possible global features in the distribution of iron, we studied the section of the Upper Cretaceous deposits in Kopet Dagh (Turkmenia) near the Kara-Kala settlement. The Kara-Kala section is located approximately 1000 km southeast from the Aimaki section (Fig. 1). It originates southward of the Isak Mountain and extends along the road between the Kyzyl-Arvat and Kara-Kala settlements. Lithologically, the section is divided into two parts. The lower part of the Cenomanian age is predominantly terrigenous. In the upper Turonian–Maastrichtian part, carbonates prevail. In this section, all stages, substages, and zones, described by A.A. Atabekyan and A.A. Likhacheva [Atabekyan and Likhacheva, 1961], are observed.

The Cenomanian deposits conformably overlying the Albian are presented by sandstones, aleurolites, and clays. Their thickness is 734 m. The Lower Turonian is lithologically similar to the upper horizons of the Cenomanian and is linked with it through gradual transition. Two members are distinguished in the Upper Turonian strata: the lower one composed of marls and the upper one presented by calciferous sediments. The substages are separated by a gap; their irregular and uneven interface is covered by glauconite grains forming a continuous crust. The thickness of the Turonian deposits is 13 m. The Coniacian rocks transgressively overlie the Turonian and are composed of red marls interbedded with gray shaly limestones and the alternation of greenish-gray clays and pink marls. This 97-m-thick sequence is conformably overlaid by the Santonian unit presented by alternating gray, pink and red marls, limestones and clays. Its thickness is 305 m. The Santonian deposits are gradually changed by the Campanian sequence formed by alternating marls and greenish-gray and white limestones 559 m thick. The Maastrichtian formation is composed of marls with a thickness of 206 m. The Maastrichtian sediments are overlapped (with traces of washout) by the Danian deposits presented by the light gray detrital and aleurite ball limestones with the iridium horizon in the bottom part. In the Danian sequence, only the lower 19 m are sampled.

The iron content in the Kara-Kala sediments is substantially higher than in the sediments of the Caucasus (Figs. 8a and 8f); it is found in 98 of 181 tested samples. The Curie points of iron vary from 690°C to 780°C (Fig. 8g). The mean Curie temperature is T_c = 740°C, which corresponds to a nickel impurity of up to 19%, and on average is 7.3%. The traces of Ni–Fe alloy are detected only in three samples (Table 3).

Besides several point excursions, also intervals of increased iron content are identified at 1845–1169 m (Cenomanian–Turonian, 99–90 Ma), 1080–1069 m (Santonian, 86.1–85.8 Ma), 720–705 m (Campanian, 82.5–82.1 Ma), and 4.5–10 m (Danian, 65–64.3 Ma). The sharp drop at 1069 m (85.8 Ma) repeats that in the data for the Caucasus and, likely, reflects the upper boundary of the Dzhalal chron. The highest iron content across all studied sections was revealed in the Cenomanian Kara-Kala deposits, where it attains 0.05%.

Similar to the Caucasian Upper Cretaceous deposits, the sediments of the Kara-Kala section are abundant with magnetic phases with T_c varying from 80°C to 450°C, magnetite (both the not oxidized (more frequently) and the cation-deficient (less frequently)), and titanomagnetite with T_c = 410–550°C. The distribution of magnetite (+ titanomagnetite) throughout the section is rather uniform (Fig. 8b). The gap is noted at a depth of 1250–1170 m (94–90 Ma, the upper parts of the Cenomanian–Turonian succession), which coincides with the decrease in the content of paramagnetic minerals (Fig. 8c). Similar depletions in the content of paramagnetic minerals are recognized in the interval 0–300 m and about 700 m (Fig. 8c). The changes in the contents of magnetite and paramagnetic minerals are not reflected in any lithological variations. Generally, the contents of magnetite and paramagnetic minerals are positively correlated (r = 0.63, Table 4), and the smooth decrease in their contents perceived from the bottom upwards (Figs. 8b and 8c) is followed by a smooth increase in M_t/M_0 ratio (Fig. 8d).

In the bottom half of the section, the iron content correlates with the content of magnetite and paramagnetic minerals (Figs. 8a, 8b, and 8c), which indicates a significant role of redeposition in the distribution of iron in these sediments. At the same time, no such correlation is found for the upper half of the section; rather, an inverse correlation is present here, which is most prominent within 80–72 Ma where practically no iron was detected (Figs. 8a, 8b, and 8c).

In several intervals of the section, "pyrit" is abundant (Fig. 8e). An intriguing feature is the antiphase occurrence of "pyrite" and titanomagnetite: from the total number of samples (181), only in 10 cases "pyrite" and titanomagnetite with T_c = 410–550°C were found to be jointly present in the sample. At the same time, in 70 cases, where titanomagnetite was present, there was no "pyrite", and in 27 cases, where "pyrite" was found, titanomagnetite was lacking. The presence of "pyrite" does not correlate with any of the other components in question (Table 4).

The Crimea Seeking possible regional correlations in the distribution of iron, we also studied the Crimean sections of the Cretaceous deposits of Verkhorech'e (the Barremian–Aptian Stage) and Sel'bukhra (the

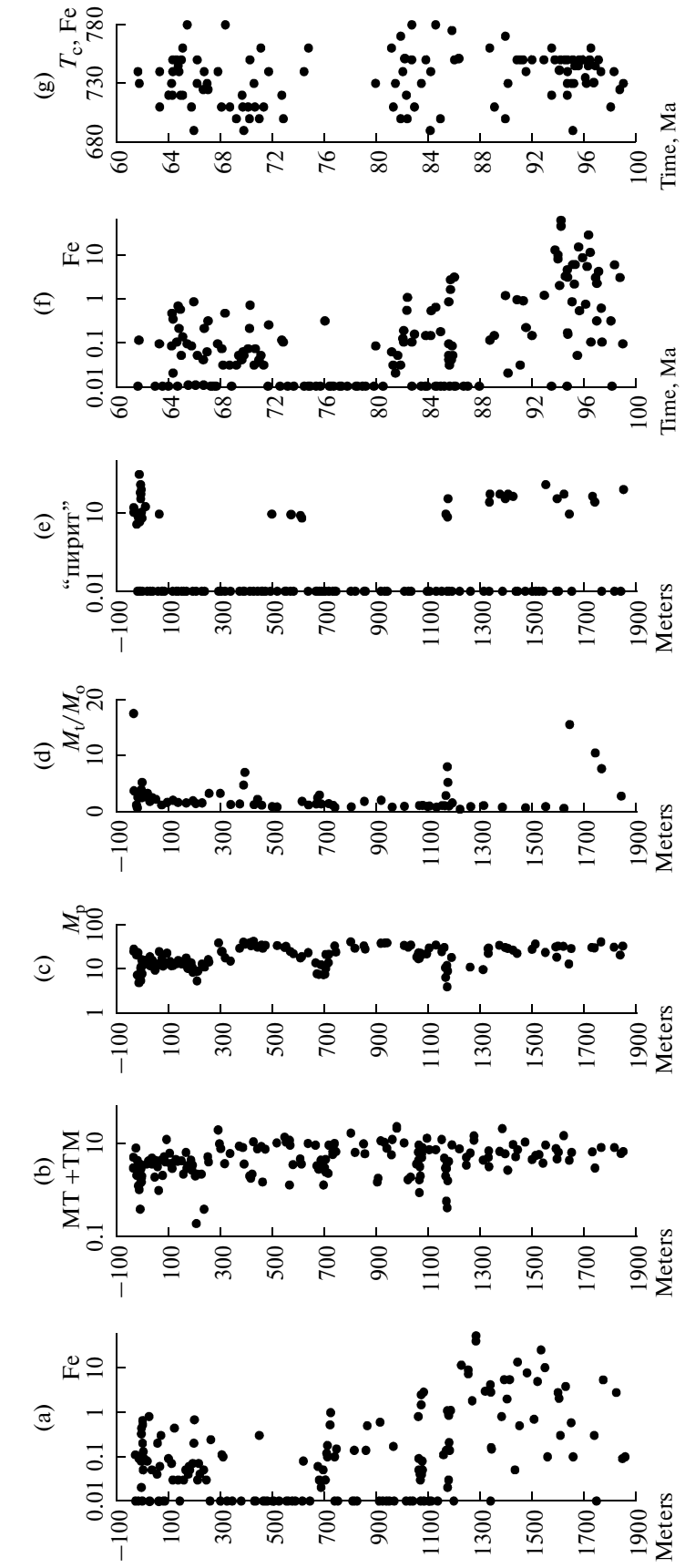

Fig. 8. The Kara-Kala column: (a) iron content, 110^{-3}%; (b) content of magnetite + titanomagnetite, 10^{-3}%; (c) fraction of paramagnetic magnetization M_p, $10^{-3}A^2/kg$; (d) the ratio of the magnetization value after the heating of the sample up to 800°C to its initial value; (e) the amplitude of the peak in the TMA curve for 510–530°C (the percentage relative to the initial magnetization of the sample), which reflect the formation of magnetite when "pyrite" is oxidized as a result of the heating of the sample; (f) and (g) the time distributions of the iron content and of the Curie points of iron, respectively.

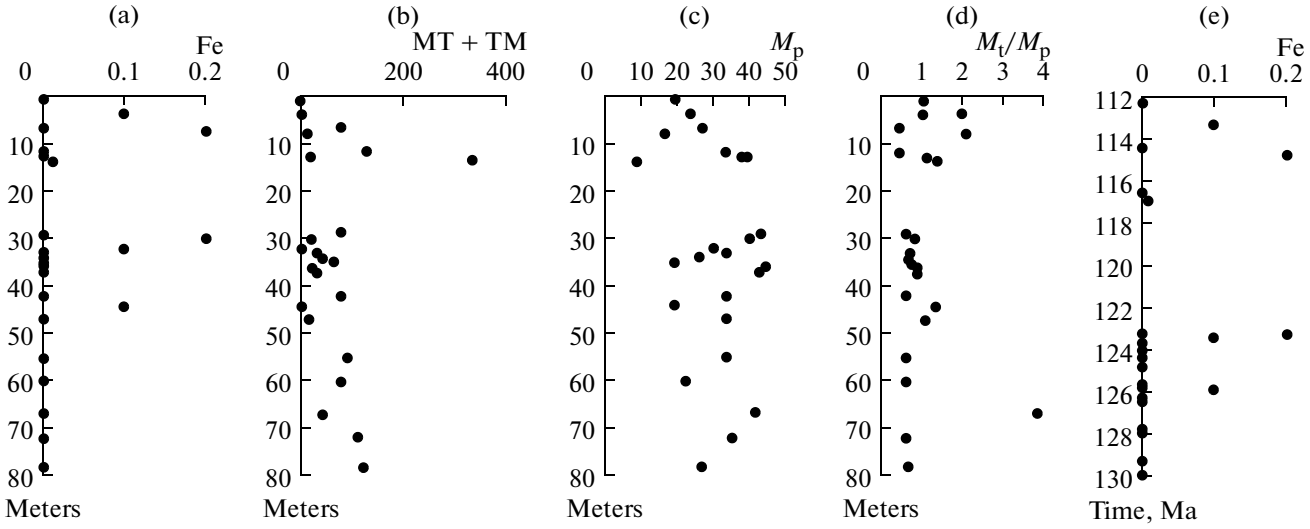

Fig. 9. The Verkhorech'e column: (a) iron content, 10^{-3}%; (b) content of magnetite + titanomagnetite, 10^{-3}%; (c) the fraction of paramagnetic magnetization M_p, $10^{-3}A^2/kg$; (d) the ratio of the magnetization value after the heating of the sample up to 800°C to its initial value; (e) the time distribution of iron contents.

Cenomanian Stage) (Fig. 1) in addition to the Kara-Kala section.

Verkhorech'e. The section of the Barremian–Aptian deposits of the Mountainous Crimea starts on the southern slope of the mountain Belaya 500 m westward from the Verkhorech'e village. With an overlap of 2–3 m, it is overbuilt by the section located 300 m nearer to the village. In the composite section, eight members are distinguished from bottom upwards [Baraboshkin et al., 2004].

Member I is the interbedding of gray and red-brown clays.A hardground-like surface is recognized in the roof of the underlying limestones; at the bottom of the clays, fine limestone pebbles and an interlayer of iron clay are present. The thickness of the unit is 6.8 m.

Member II is composed of gray, yellow-gray, and in the upper part brown clays interbedded with cherry-red ankerites. The thickness of the unit is 7.5 m.

Member III is presented by an alternation of bioturbated gray clays with scattered concretions of sulfides and brownish-gray clays. The thickness of the unit is 8.3 m.

In Member IV, gray clays alterating with brownish clays with rare interlayers of cherry-red ankerite concretions are observed. The apparent thickness of the sequence is approximately 32 m; the overlying part is turfed.

Member V is clay with separate bright green spots and stains. The thickness of the unit is 5.5 m.

Member VI is composed of gray bioturbated clay with fine brownish-beige phosphate nodules at the bottom. The thickness of the layer is 3.5 m.

In Member VII, red clay, which is finely interbedded with greenish-gray clay in the lower part of the layer, is changed upwards by brown bioturbated clay; concretions of cherry ankerite are present at the bottom. The thickness of the unit is 3.1 m.

Member VIII is composed of gray bioturbated clay with a thickness of 3 m.

Members I–IV (the bottom part) refer to the Barremian, members IV (the upper part) and VIII, to the Aptian. A noticeable part of the Aptian sequence between 19 and 29 m (123–117 Ma) is absent.

The deposits of Verkhorech'e are almost devoid of iron and Ni–Fe alloy (Figs. 9a and 9e): no reliable determination of these species is provided by TMA tests. At places, insignificant concentrations of iron are detected; there, its Curie point varies from 720°C to 780°C, which indicates that this is iron with 12% to zero nickel. Similar to the Caucasian Cretaceous deposits, in the sediments of Verkhorech'e, the magnetic phases with the Curie temperature T_c varying from 80°C to 450°C, the magnetite (predominantly cation-deficient) and titanomagnetite with $T_c = 410$–550°C are pervasive. The Verkhorech'e section is characterized by increased contents of paramagnetic minerals and magnetite, which exceed those in the sand-shale deposits of Gergebil' and Kara-Kala (Figs. 9b and 9c). The inverse correlation between the contents of paramagnetic minerals and magnetite (Table 4) is an unusual feature of this section, which distinguishes it from the other sections.

Sel'bukhra. The Sel'bukhra section is located in the Bakhchisarai region of the Mountainous Crimea in the neighborhood of Prokhladnoe village. The Cenomanian deposits outcrop on the southern slope of Mt. Sel'bukhra. The detailed description of the section is presented in the paper [Alekseev et al., 1997]. The Cenomanian deposits unconformably overlie the Upper Albian sandstones. The lower part of the Lower

Cenomanian is composed of sandstones and aleurolites, and its upper part is formed by an alternation of dark clay and bright calcareous marls. The gravel conglomerate with quartz gravel and glauconite is recognized at the bottom. The thickness of the sequence is 19 m. The Middle Cenomanian formations are presented by dark gray marls with limestone interbeds; higher up in the succession, they pass into the sequence of rhytmical alternation of light grey limestones and dark gray clay marls with rare concretions of sulfides. The interface with the Lower Cenomanian is expressed by the hardground. The thickness of these deposits is 16 m. The Upper Cenomanian is composed of marls and white limestones. A thin interlayer of bentonitic clays is identified on the contact with the Middle Cenomanian. The visible thickness of the Upper Cenomanian is 16 m.

Iron was discovered in 27 of 36 samples tested (Fig. 10a), and only in two of them the signs of Ni–Fe alloy were found (Table 3). At the bottom of the section, the iron content is approximately 3×10^{-3}%, dropping upwards along the section by over two orders of magnitude. The Curie points of iron vary from 780°C to 780°C (Fig. 10f), the mean Curie temperature is $T_c = 745$°C; i.e., the nickel percentage reaches 17% and is 6% on average.

The magnetic phases with the Curie temperature T_c varying from 80°C to 400°C, magnetite (rarely, cation-deficient magnetite), titanomagnetite with T_c = 410–550°C, and hematite are pervasive throughout the section. The content of magnetite (+ titanomagnetite) in the sandstones at the bottoms of the section attains 0.3% and smoothly decreases from bottom to top across the section (Fig. 10b). The behavior of magnetite is echoed in the content of paramagnetic minerals (Fig. 10c) and in the iron content (Fig. 10a). A noticeable positive correlation is observed between all three magnetic phases (Table 4). Such a similar behavior of iron, magnetite and paramagnetic minerals across the section suggests that redeposition played a significant role in the accumulation of iron in the sediments of Sel'bukhra.

RESULTS AND DISCUSSION

The content of metallic particles in the sediments. The studied sediments are abundant with particles of metallic iron. The latter are identified in 330 of 571 studied samples in concentrations ranging from 10^{-5}% to 0.05%. Similar distributions are also observed in the Cretaceous to the Miocene sections in Austria, Russia (the Volga Region), Georgia, and Turkmenia [Pechersky, 2008; Pechersky et al., 2008; Grachev et al., 2009].

The appearance and accumulation of iron does not depend on the oxidation-reduction conditions in sediments, which is shown by the lack of correlation of iron with the presence of cation-deficient magnetite (the high-oxidizing conditions), on the one hand, and "pyrite" (the reducing conditions), on the other hand, in the sediments.

Generally, both the individual sections and regions and the aggregate data exhibit bimodal distribution of the iron particles concentrations (Fig. 11), which reflects their heterogeneous accumulation in the sediments. One pool of data with the "zero" mode is the sediments devoid of iron (iron has not been detected by TMA). The distribution of such sediments in the studied sections is irregular. Another data set is characterized by lognormal distribution with the mode in the interval $0.04–0.15 \times 10^{-3}$%. Here,the mode for the deposits from the Dzhalal hyperchron (the Aptian–Santonian Stage) is somewhat higher, compared to that for the younger deposits (Fig. 11). The Kara-Kala sediments stand out against the general background by the "tail" of increased concentrations (Fig. 11b).

Thus, we observe rather geographical than lithological control: the iron content increases west-to-east. The Cretaceous deposits of the Crimea are very poor in iron; this regards both the sandy-argillaceous sediments (except for the very bottoms of the Cenomanian unit of the Sel'bukhra section where the local content is 0.003%) and the carbonate deposits, where it is at most $0.1–0.2 \times 10^{-3}$%. The Upper Cretaceous carbonate deposits of the Caucasus contain more iron: here its content attains $0.5–10 \times 10^{-3}$%. Local anomalies as high as $0.5–3 \times 10^{-3}$% are revealed in the sandy-argillaceous Lower Cretaceous Gergebil' deposits. The highest iron contents are observed in the East, in the Kara-Kala section, where it attains 0.05% in the Cenomanian section of the sequence.

As shown by the lack of correlation between the content of extraterrestrial iron with the terrestrial magnetite + titanomagnetite (Table 4), the main sources of the iron accumulated in the discussed sediments were directly the space sources. The exceptions are the Cenomanian Sel'bukhra and Kara-Kala deposits, where a noticeable correlation of iron content with the content of magnetite (Table 4) most probably indicates that redeposition was an important factor contributing to the accumulation of iron in the Cenomanian sediments of these regions.

Here, we may speak about four types of the accumulation of metallic iron: dotty, local, regional, and global.

The dotty type is most common. In this type of accumulation, the increased iron content is identified in an individual sample (at a point, or as a dot) and is absent in the adjacent samples. This type has a random character. It is possibly the result of either the primary entry of iron in the sediments or its redeposition.

The local type is characterized by the increased iron content detected in a series of neighboring samples of one section, although not traceable from one section to another. Most likely, this is a combination of primary accumulation and secondary redeposition. The most striking example of the long-term irregular local

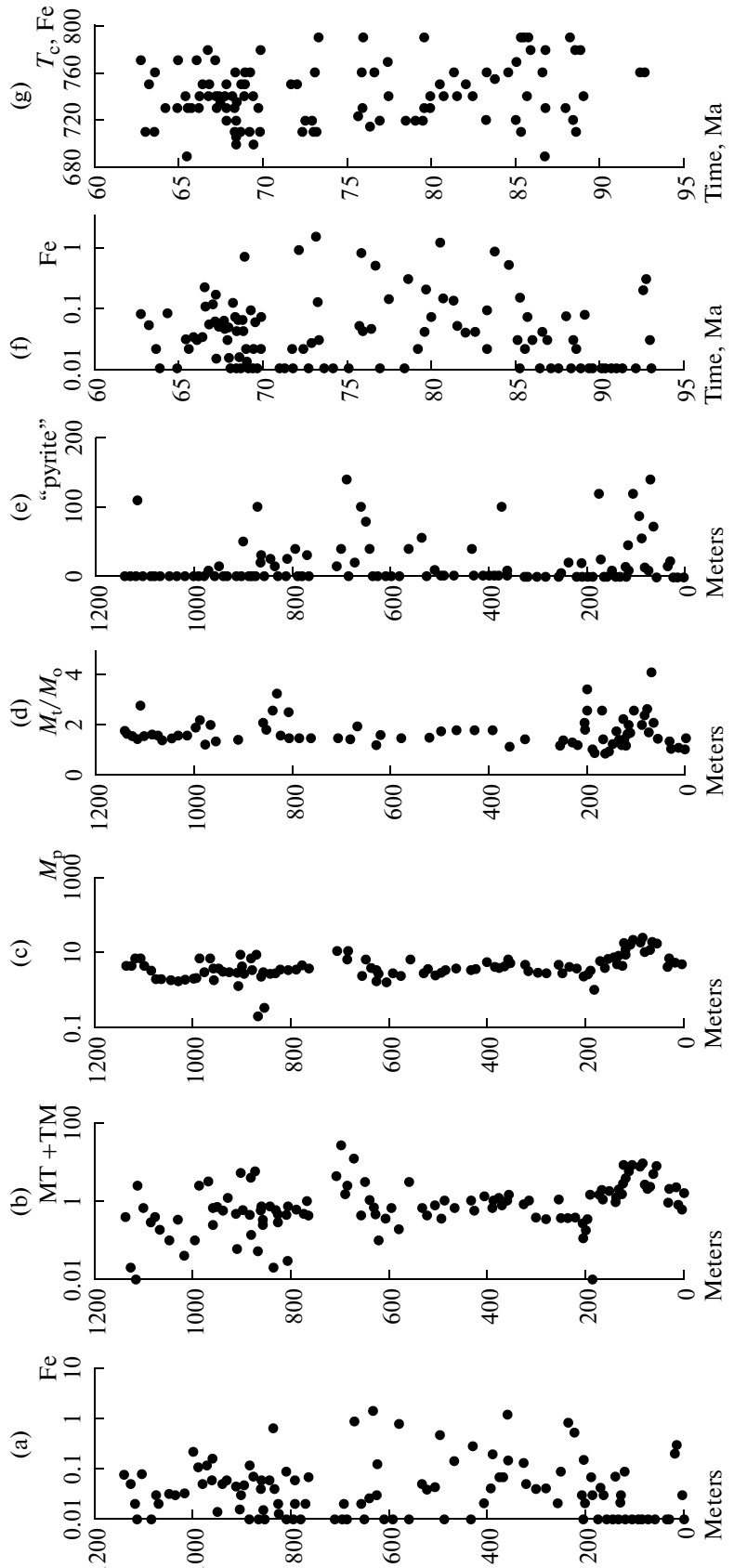

Fig. 10. The Sel'bukhra column: (a) iron content, 10^{-3}%; (b) content of magnetite + titanomagnetite, 110^{-3}%; (c) fraction of paramagnetic magnetization M_p, 10^{-3} A^2/kg; (d) the ratio of the magnetization value after the heating of the sample up to 800°C to its initial value; (e) the amplitude of the peak in the TMA curve for 510–530°C (the percentage relative to the initial magnetization of the sample), which reflects the formation of magnetite when "pyrite" is oxidized as a result of the heating of the sample; (f) and (g) the time distributions of the iron content and of the Curie points of iron, respectively.

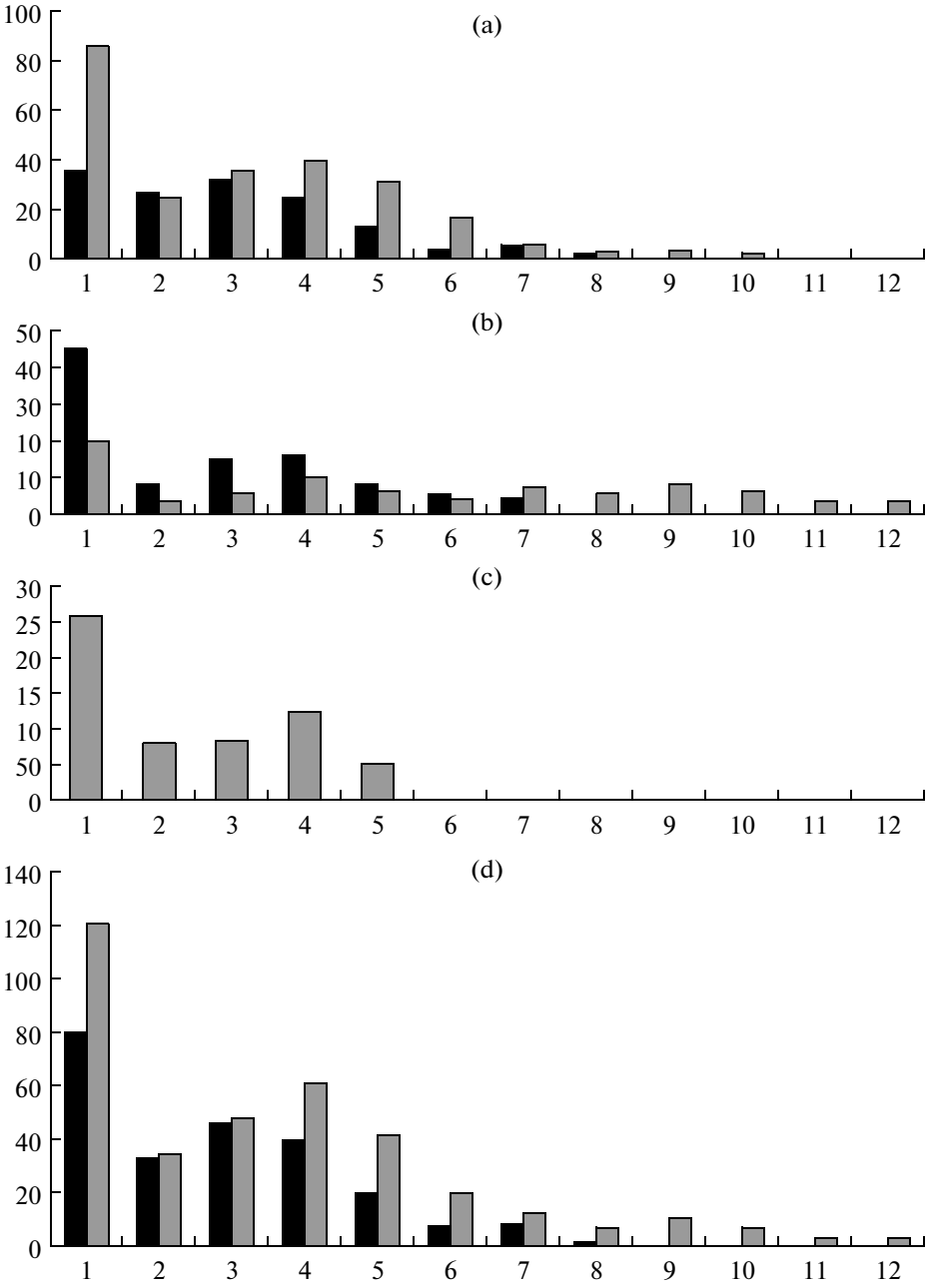

Fig. 11. Histograms of the iron concentration in the sections of (a) the Caucasus, (b) the Kara-Kala and (c) the Crimea. The Campanian–Danuian deposits (younger than the Dzhalal hyperchron) are shown in black, the Barremian–Santonian deposits (coeval with the Dzhalal hyperchron) are shown in gray. The intervals of iron contents are shown on the logarithmic scale: (1) 0–0.01(10^{-3}%); (2) 0.01–0.03; (3) 0.03–0.07; (4) 0.07–0.15; (5) 0.15–0.31; (6) 0.31–0.63; (7) 0.63–1.27; (8) 1.27–2.55; (9) 2.55–5.11; (10) 5.11–10.23; (@11) 10.23–20.49; (2) 20.49–54 (10^{-3}%).

primary accumulation of iron (the metallic iron is not correlated with the terrestrial iron minerals) is the Bass section in the interval from 81 Ma to 72 Ma (Fig. 7, Table 4). An example of long-term predominantly secondary accumulation of iron as a result of redeposition is the Kara-Kala section (95–99 Ma), where the correlation between the iron content exhibits a noticeable correlation with terrestrial minerals (Table 1), especially in the lower part of the section (Fig. 8). In the lower part of the Dzhalal hyperchron, in the Gergebil' section, a number of local spikes of iron content attaining $2–3 \times 10^{-3}$% is detected at the ages of 107.54 Ma, 116.17 Ma and 128.08 Ma. Possibly, after the study of a series of the Lower Cretaceous sections in the other regions, part of these increases will prove to be regional.

In **the regional type,** the increased iron content is identified in the coeval intervals in a series of sections,

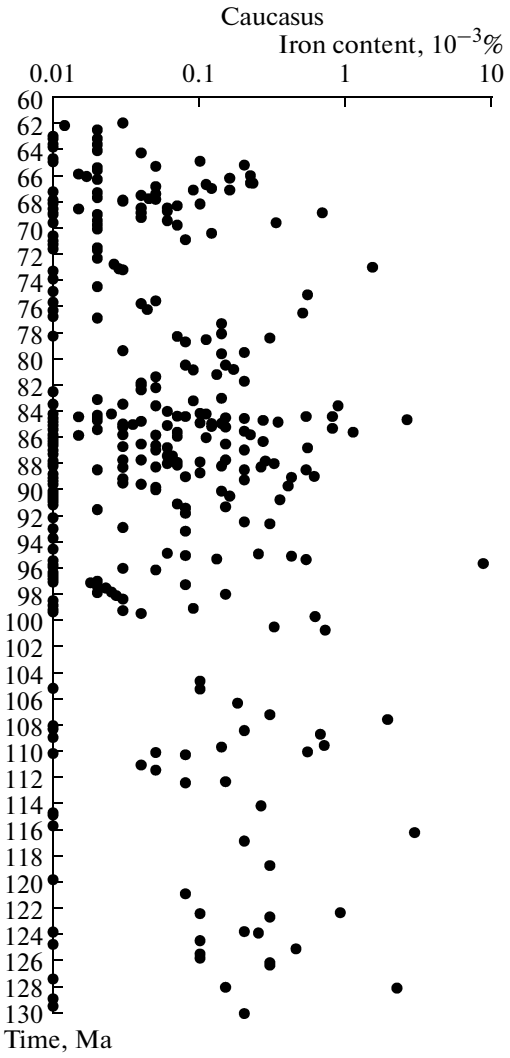

Fig. 12. Distribution of iron particles in the sediments of the Caucasus. The aggregated data for the Aimaki, Dzhengutai, Madzhalis, Gergebil', and Bass sections compiled in a single column.

for example, of the Caucasus. These enhancements are unlikely the results of redeposition, which was synchronous across a large territory. If we compile all sections of the Caucasus, we should obtain a more distinct pattern of regional enrichment of sediments with iron; the dotty and, probably, the local values will be smoothed out, as will also be smoothed the effect of secondary redeposition (Fig. 12).

In our opinion, the most prominent intervals of **regional** accumulation of iron are the following:

(1) 64 Ma–67 Ma, the lower Danian–upper Cretaceous; the iron content approaches 10^{-3}% and is identified in all studied sections where this interval of ages is present (Figs. 3, 7, 8, and 12).

(2) 84 Ìà–86 Ìà, the Santonian, the iron is detected in five sections, the maximum iron content varies from one section to another from 0.2×10^{-3}% (Madzhalis, Fig. 5) up to 2.9×10^{-3}% (Kara-Kala, Fig. 8). The limits of the interval somewhat vary, which is probably connected with the uncertainty of transition from the stratigraphic scale to the chronological scale. It is particularly interesting and important that this interval practically coincides with the upper boundary of the Dzhalal hyperchron. In the composite section (Fig. 12), this boundary is clearly outlined by the drop in the iron content near 84 Ma. The lower boundary of the Dzhalal hyperchron is not clearly distinguished (Fig. 12) since the amount of data is insufficient. Possibly, the decrease in the iron content at the level of 122 Ma refers to the lower boundary of the Dzhalal hyperchron.

(3) 94 Ma–96 Ma, Late Cenomanian, iron is identified in the Aimaki section (the maximum content 9×10^{-3}% corresponding to the age of 95.6 Ma), and in the Kara-Kala section (the maximum attaining 54×10^{-3}% corresponding to 94.3 Ma). By stretching a point, this might be attributed to the regional accumulation of iron due to the noticeable role of secondary redeposition of iron in the lower parts of both sections (Table 1, Figs. 3, 8, and 12).

The global type of accumulation implies that increased iron content is found in the coeval sediments of sections located at large distances from each other. The accumulation of iron near the upper boundary of the Dzhalal hyperchron (the Santonian Epoch) can be related to this global type.

The generally pervasive occurence of iron particles suggests that their main source is cosmic dust. Precipitation of the iron particles to the Earth is irregular; this fact, apparently, reflects the different sources of iron particles in the dust, which is shown by the bimodal distribution of their concentrations (Fig. 11).

In contrast to the iron particles, the particles of Ni–Fe alloy are very rare, and their number does not correlate with the content of iron particles ($r = -0.059$). Their noticeable correlation with the content of magnetite and titanomagnetite in the sediments ($r = 0.61$) implies that a part of these particles is not Ni–Fe alloy but rather terrestrial minerals such as titanomagnetite and hemoilmenite, which are fully preserved upon heating up to 800°C (which is barely probable); or it is the particles of Ni–Fe alloy redeposited together with the terrestrial minerals. Such a sharp difference in the amount and the conditions of accumulation of the particles of iron and Ni–Fe alloy and lack of correlation of their contents is most likely due to their different sources. The former are mainly the products of the cosmic dust precipitation onto the Earth, while the latter are more probably associated with impact events. In any case, regardless of the reliability of our proposed method for identifying the particles of the Ni–Fe alloy, we can unambiguously assert that cosmic dust is practically void of particles of Ni–Fe alloy, or, in more exact terms (at the threshold of TMA sensitivity), the possible concentration of these particles in the dust cloud is below 10^{-5}%.

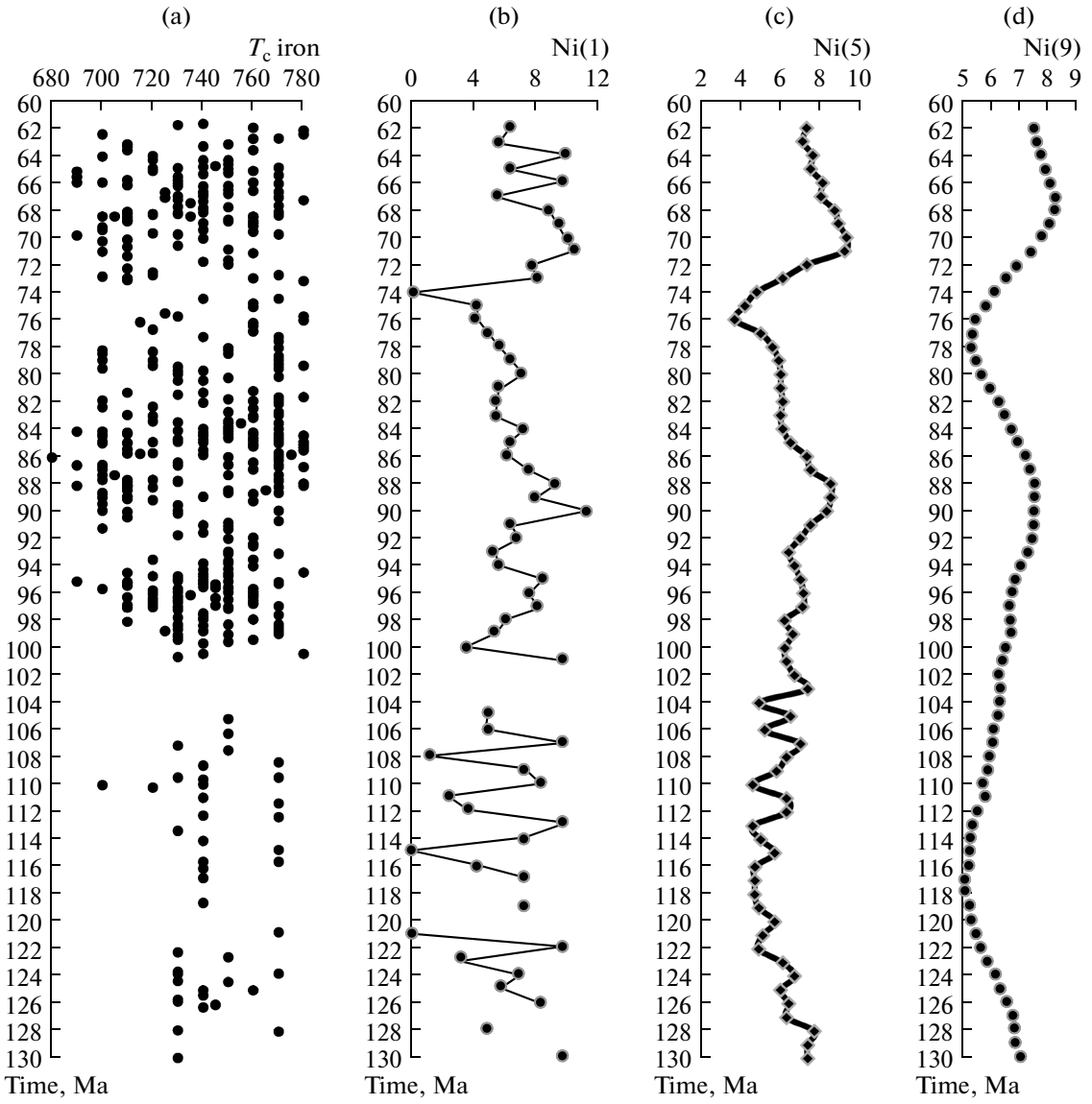

Fig.13. (a) Distribution of the Curie points in the composite Caucasus–Kara-Kala section; (b) conversion of the Curie points into the nickel content (%) in the iron particles, the interval of averaging is 1 Ma; (c) the same as (b), the interval of averaging is 5 Ma; (d) the same as (b), the interval of averaging is 9 Ma.

Composition of metallic particles. The composition of iron particles, expressed in terms of their Curie points, in all sections varies within approximately similar limits from 680°C to 780°C, which corresponds to 22% to zero nickel content. The upper limit of the nickel content (22%) is conventional and is determined by the fact that at higher concentrations the Curie points of Fe–Ni alloy overlap with the Curie points of hematite, magnetite, hemoilmenites, and titanomagnetites. Although their separation is possible, it requires special experiments, which are beyond the scope of our study. To date, a series of samples was selected, which, possibly, contain particles of Ni–Fe alloy with the Curie points ranging from 360°C to 500°C. The nickel content in such particles varies from 67 to 100% (Table 3). Our determinations of Ni–Fe alloy are possibly not free of errors, therefore, the true number of samples containing Ni–Fe alloy is probably even less.

The lateral distribution of the Curie points of iron (between the sections) exhibits no distinct regularity (Figs. 3–8): the composition of iron particles form a large cloud, which is, probably, natural for cosmic dust. In the composite plot in Fig. 13a, two intervals are distinguished, approximately 130–105 Ma and 78–74 Ma, in which the lower limit of the Curie points is above (720–730°C) and, thus, the nickel content is below their corresponding values in the other geological time intervals. This is better seen from the TMA data recalculated into the nickel content in the iron particles and averaged (Figs. 13b, 13c, and 13d). The regular trend (Fig. 13d) becomes more distinct as the

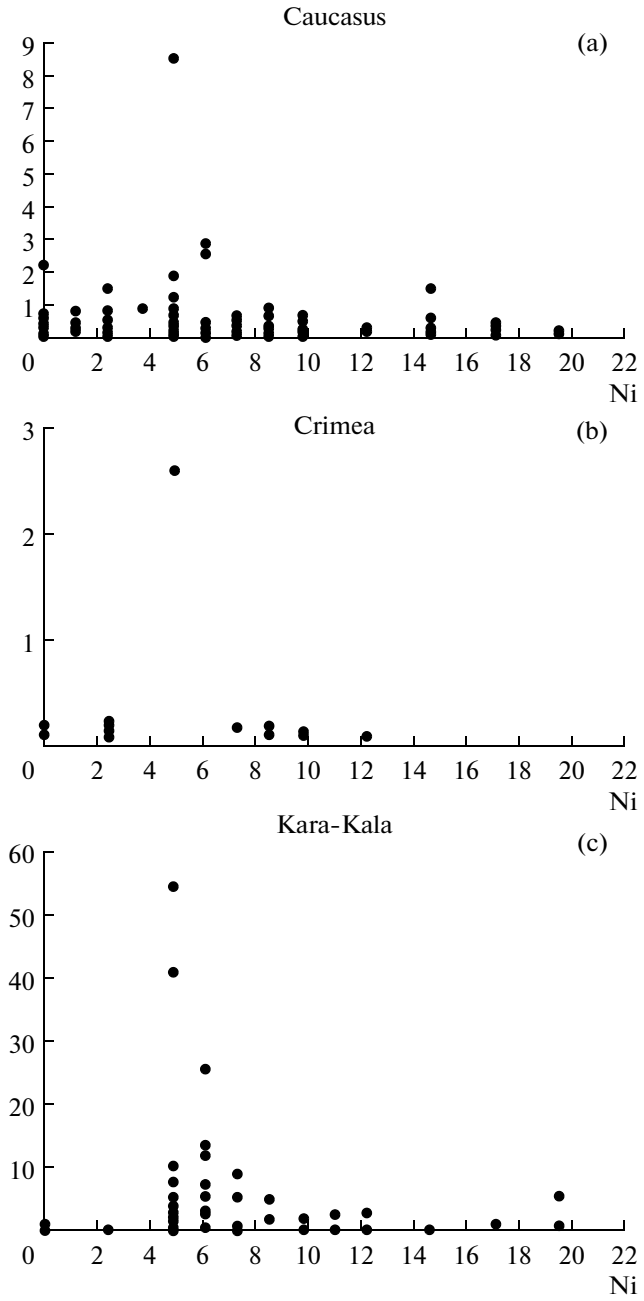

Fig. 14. Nickel content (%) in the iron particles (10^{-3}%): (a) the Caucasus, (b) the Crimea, (c) the Kara-Kala.

degree of smoothing increases: the drop in the average content of nickel in the interval from 130 to 124 Ma followed by a fairly weak smooth growth up to 87 Ma changes by a new decrease up to 78 Ma, a new growth up to 68 Ma, and a subsequent decrease to 60 Ma. There is a noteworthy interval with almost constant average nickel content, which practically ***coincides with the Dzhalal hyperchron***; its lower and upper boundaries are marked by the decrease in the nickel content in the particles of iron. Such regular behavior of the average composition of the iron particles clearly characterizes the iron particles precipitated from a cloud of cosmic dust through which our planet was passing at that time. The composition of iron particles, on average, smoothly and uniformly varies in time. In contrast to the total iron content in sediments, which is affected by probable redeposition, the latter has no effect on the composition of grains of iron.

There is no correlation between the concentration of iron particles and the nickel content in them ($r = -0.024$). At the same time, there is a distinct peak of the increased iron content with a practically constant nickel impurity of 5% seen in Fig. 14, which persists regardless of the place and the age of sediments containing this iron. An increased concentration of iron with nickel impurity of precisely 5% is noted even in the Crimean sediments, which are poor in iron (Fig. 14c). Thus, this is a certain global effect. The iron content in the sediments rapidly drops towards either an increase or a decrease in the nickel content (Fig. 14a). There is a regional specific feature, though: the Kara-Kala sediments are practically void of grains of iron with nickel content below 5%, whereas the Crimean and especially the Caucasian sediments contain a noticeable fraction of grains with less than 5% nickel up to pure iron.

CONCLUSIONS

With the aid of thermomagnetic analysis up to a temperature of 800°C, we obtained a detailed distribution of metallic iron particles in space and time in the Cretaceous and Danian deposits, which was impossible to achieve using the methods of direct observation.

The main results of our studies can be summarized as follows.

(1) The particles of metallic iron in concentrations from 10^{-5}% to 0.05% are common both in the studied sediments and in the sections of Austria, Russia (the Volga Region), Georgia, and Turkmenia, covering the period from the Cretaceous to the Miocene. Irrespective of the age of the deposits, the distribution of the metallic iron is bimodal. The first pool of samples with the zero mode includes sediments, in which iron is absent (not detected by TMA); the distribution of such sediments in the studied sections is irregular, which likely reflects the nonuniform entrance of iron particles into the sediments. The second set has a lognormal distribution with the mode of 0.04–0.15 (10^{-3}%).

(2) The regional enrichment with iron particles is detected in the Santonian sediments in the interval of approximately 84 Ma–86 Ma in five sections of the Caucasus and in the Kara-Kala section, which are spaced 1000 km apart from each other. The maximum iron content varies from one section to another from 0.2×10^{-3} to 2.9×10^{-3}%. The upper boundary of this interval practically coincides with the upper boundary of the Dzhalal hyperchron and is outlined by the drop in iron content near 84 Ma.

(3) The variations in the composition of iron particles manifest themselves in their Curie points. In all

sections, either the Cretaceous or the Danian and Miocene, the latter vary from 690°C to 780°C following the fluctuations in the nickel content, which likely characterize the fluctuations in the composition of the iron particles in the cosmic dust cloud. Upon smoothing, *the interval of 123–86 Ma with almost constant average nickel content becomes clearly distinguished. This interval practically coincides with the Dzhalal hyperchron and its lower and upper boundaries are marked by a drop in the nickel content in the iron particles.*

(4) In all studied sections, against the very low background concentrations of iron particles with noticeably varied nickel content, there is a peak of increased iron content with practically constant nickel percentage (5%), irrespective of the locality and the age of the sediment containing this iron, i.e., this is a certain global effect.

(5) The global distribution and the duration of episodes of increased iron content in the sediments, and nearly constant nickel content, most likely, characterize the cosmic dust cloud through which the Earth passed at that time.

(6) In many sections of Cretaceous and Cenozoic sediments studied by us, particles of Ni–Fe alloy and pure nickel are very rare, and their concentrations do not correlate with the content of iron particles. Such a sharp difference in the amounts and the accumulation conditions between the particles of iron and Ni–Fe alloy is most likely explained by their different sources. The iron particles are mainly the products of precipitation of cosmic dust onto the Earth, while the particles of Ni–Fealloy are probably related with the impact events. Anyway, regardless of the reliability of our proposed method for identification of particles of Ni–Fe alloy, we may unambiguously state that the probable concentration of the particles of Ni–Fe alloy in cosmic dust is below 10^{-5}% (at the threshold sensitivity of TMA).

REFERENCES

Alekseev, A.S., Vengertsev, V.S., Kopaevich, L.F., and Kuz'micheva, T.A., Lithology and Micropaleonthology of the Cenomanian–Turonian Boundary Deposits in the Southwestern Crimea, in *Trudy Krymskogo geologicheskogo nauchno-uchebnogo centra im. Bogdanova* (Proceedings of the Crimean Bogdanov Geological Scientific–Educational Center), 1997, vol. 1, pp. 54–73.

Atabekyan, A.A. and Likhacheva, A.A., The Upper Cretaceous Deposits of the West Kopet Dagh, in *Problemy neftegazonosnosti Srednei Azii. Tr. VSEGEI* (The Problems of the Oil and Gas-Bearing Capacity of the Central Asia. Proc. VSEGEI), Leningrad: Gostoptekhizdat, 1961, vol. 62, no. 10.

Baraboshkin, E.Yu., Guzhikov, A.Yu., Mutterlouz, Y., Yampolskaya, O.B., Pimenov, M.V., and Gavrilov, S.S., The New Data on the Stratigraphy of the Barremian–Aptian Deposits of the Mountaineous Crimea in Connection with Identification of the Analog of M_0 Chron in the Section of Verkhorech'e Village, *Vestn. Mosk. Univ., Ser. 4: Geol.*, 2004, no. 1, pp. 10–20.

Bozorth, R.M., *Ferromagnetism*, New York: Van Nostrand, 1951.

Brownlee, D.E., Morphological, Chemical and Mineralogical Studies of Cosmic Dust, *Phil. Trans. Roy. Soc. London*, 1987, vol. À323, pp. 305–309.

Burov, B.V., Nurgaliev, D.K., and Yasonov, P.G., *Paleomagnitnyi analiz* (Paleomagnetic Analysis), Kazan: KGU, 1986.

Diagrammy sostoyaniya dvoinykh metallicheskikh sistem (State Diagrams for Binary Metallic Systems), Lyakisheva, N.P., Ed., Moscow: Mashinostroenie, 1997, Book 1, vol. 3.

Grachev, A.F., Korchagin, O.A., Kollmann, H.A., et al., The K/T Boundary of Gams (Eastern Alps, Austria) and the Nature of Terminal Cretaceous Mass Extinction, in *Abhandulgen der Geologischen Bundesfhstalt*, Vien, 2009, pp. 1–199.

Gradstein, F.M., Ogg, J., and van Kranendonk, M., On the Geological Time Scale 2008, *Newsletters on Stratigraphy*, 2008, vol. 43, no. 1, pp. 5–13.

Melovye otlozheniya obramleniya Kaspiiskogo morya (Cretaceous Deposits of the Caspian Sea Margins), Moscow: Nauka, 1980.

Nagata, Ò., Danon, J., and Funaki, M., Magnetic Properties of Ni-Rich Iron Meteorites, *Mem. Natl. Inst. Polar Res. Spec. Issue*, 1987, vol. 46, pp. 263–282.

Nagata, T. and Funaki, M., Tetrataenite Phase in Antarctic Meteorites, *Memory Natl. Inst. Polar Res., Spec. Issue*, 1987, vol.46, pp. 242–251.

Nagata, Ò., Ishikawa, Y., Kinoshita, H. et al., Magnetic Properties of Lunar Samples, *Science*, 1970, vol. 167, pp. 703–722.

Novakova, A.A. and Gendler, T.S., Metastable Structural-Magnetic Transformations in Sulfides in Course of Oxidation, *J. Radioanalyt. Nuclear Chem.*, 1995, vol. 190, no. 2, pp. 363–368.

Parkin, D.W., Cosmic Dust in Antarctic, *Br. Antarctic Surv. Bull.*, 1964, vol. 23, pp. 1–18.

Pechersky, D.M., Metallic Iron in Sediments at the Mesozoic-Cenozoic (K/T) Boundary, *Russ. J. Earth Sci.*, 2008, vol. 10, p. ES6006, doi:10.2205/2005ES000304c .

Pechersky, D.M., Nourgaliev, D.K., and Trubikhin, V.M., Native Iron in Miocene Sediments, *Russ. J. Earth Sci.,* 2008, vol. 10, p. ES6004, doi:10.2208/2005ES000306c.

Pergament, M.A., Stratigraphy and Inoceramuses of the Upper Cretaceous of the Northern Hemisphere, in *Trudy GIN AN SSSR* (Proc. Geol. Inst. Acad. Sci. USSR), 1978, vol. 322.

Rengarten, V.P., *Opornye razrezy verkhnemelovykh otlozhenii Dagestana* (Reference Sections of the Upper Cretaceous Deposits of Daghestan), Leningrad: Nauka, 1975.

Shima, M. and Yabuki, H., Study of the Extraterrestrial Material in Antarctica, *Natl. Inst. Polar. Res.*, 1988, vol. 3, pp. 53–67.

The Upper Cretaceous in the South of the USSR, M. M. Aliev, N. A. Krylov, M. M. Pavlova, et al., Eds., Moscow: Nauka, 1986.